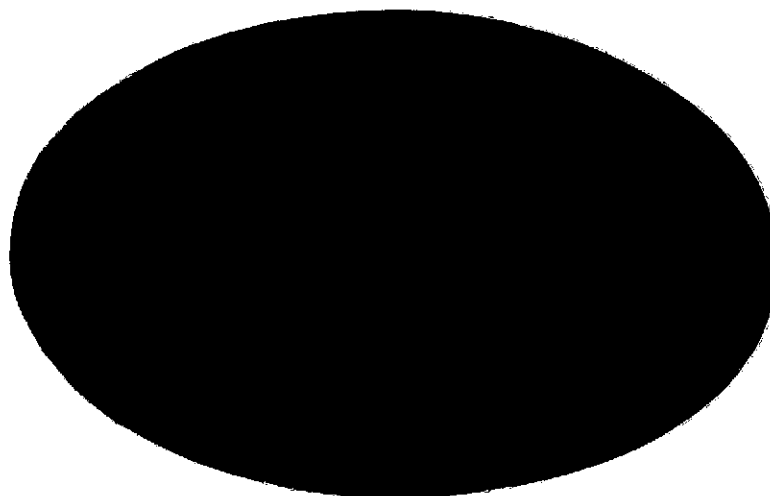


DRA



(NASA-CR-120364) BOUNDARY LAYER INTEGRAL
MATRIX PROCEDURE CODE MODIFICATIONS AND
VERIFICATIONS Final Report (Aerotherm
Corp.) 42 p HC \$5.25 CSCL-20D
N74-31752
G3/12 17058 Unclass

Aerotherm Project 6282

March 1974

Aerotherm Final Report 74-95

BOUNDARY LAYER INTEGRAL MATRIX
PROCEDURE CODE MODIFICATIONS AND
VERIFICATIONS

By

R. Michael Evans
Howard L. Morse

Prepared For

National Aeronautics and Space Administration
George C. Marshall Space Flight Center
Marshall Space Flight Center, Alabama 35812

Contract No. NAS8-29667

Technical Monitor: Klaus Gross

Aerotherm Division/Acurex Corporation
Mountain View, California 94042

ABSTRACT

A summary of modifications to Aerotherm's Boundary Layer Integral Matrix Procedure (BLIMP) code is presented. These modifications represent a preliminary effort to make BLIMP compatible with other JANNAP codes and to adjust the code for specific application to rocket nozzle flows. Results of the initial verification of the code for prediction of rocket nozzle type flows are discussed. For those cases in which measured free stream flow conditions were used as input to the code, the boundary layer predictions and measurements are in excellent agreement. In two cases, with free stream flow conditions calculated by another JANNAP code (TDK) for use as input to BLIMP, the predictions and the data were in fair agreement for one case and in poor agreement for the other case. The poor agreement is believed to result from failure of the turbulent model in BLIMP to account for laminarization of a turbulent flow. Recommendations for further code modifications and improvements are also presented.

TABLE OF CONTENTS

<u>Section</u>		<u>Page</u>
1	INTRODUCTION	1-1
2	CODE MODIFICATIONS	2-1
	2.1 Namelist	2-1
	2.2 Thermochemical Data	2-1
	2.3 Input/Output Changes	2-1
	2.4 Refit Option	2-2
3	RESULTS OF VERIFICATION ANALYSIS	3-1
	3.1 Data of Brott, Yanta, Voisinet, and Lee	3-2
	3.2 Rocketdyne: O_2/H_2 Two-Dimensional Nozzle	3-2
	3.3 SSME Model Test - 2 Hot Air	3-8
	3.4 Back and Cuffel - Supersonic Nozzle with Heat Transfer	3-12
	3.5 Summary	3-16
4	RECOMMENDATIONS	4-1
	REFERENCES	R-1
	APPENDIX A	A-1

LIST OF FIGURES

<u>Figure</u>		<u>Page</u>
3-1	Linear-Log Velocity Profiles. Brott, et al.	3-3
3-2	Momentum Thickness Reynolds Number. Brott, et al.	3-4
3-3	Skin Friction Coefficient. Brott, et al.	3-5
3-4	Comparison of Measured and Predicted Heat Flux for Rocketdyne O ₂ /H ₂ Nozzle Flow	3-7
3-5	Comparison of Measured and Predicted Mach No. Profiles, SSME Model Test ($c = 77.5$)	3-9
3-6	BLIMP Predictions for Momentum Thickness and Displacement Thickness SSME Model Test	3-10
3-7	Comparison of Reported and Predicted Velocity Profile, SSME Model Test ($c = 77.5$)	3-11
3-8	Schematic of Back and Cuffel Nozzle Showing Boundary Layer Probe Stations	3-13
3-9	Measured and Predicted Velocity Boundary Layer Profiles for Back and Cuffel Data	3-14
3-10	Momentum Thickness and Displacement Thickness for Back and Cuffel Data	3-15
3-11	Measured and Predicted Total Temperature Profiles for Back and Cuffel Data	3-17
3-12	Comparison of Mass Flux Profile for Data of Back and Cuffel	3-18
3-13	Comparison of Heat Flux Data and Predictions for Back and Cuffel Data	3-19
3-14	Comparison of Velocity Profile at $X/R_T = 10.797$ for Data of Back and Cuffel	3-20

LIST OF SYMBOLS

C_f	skin friction factor
K	laminarization parameter $(= (v_e^2/u_e) du_e/ds)$
L	length normalizing factor (locally defined)
l	length normalizing factor (locally defined)
M.R.	mixture ratio
P	pressure
\dot{Q}	heat flux
R	radius
Re_θ	Reynolds number based on momentum thickness
s	wall length
T	temperature
U	velocity
X, x	axial coordinate, 0 at the throat
y	physical coordinate normal to nozzle wall
δ	velocity boundary layer thickness
δ^*	displacement thickness $(\delta^* = \int_0^\infty (1 - \rho u/\rho_e u_e) dy)$
ϵ	area ratio

ν kinematic viscosity

ρ density

θ momentum thickness $(\theta = \int_0^{\infty} (1 - u/u_e) (\rho u / \rho_e u_e) dy)$

ϕ wall angle

Subscripts

e edge value

o stagnation value

T throat value

w wall value

SECTION 1

INTRODUCTION

Boundary layer behavior along the walls of a rocket nozzle plays an important role in the performance of the nozzle. The shear layer determines part of the thrust loss of the nozzle and the energy layer controls the heat transfer to the wall and the wall temperature. There is a well established need for a computer code which can calculate boundary layer effects for flows with large pressure gradients, chemical reactions, and a wide variety of wall conditions. To this end Aerotherm's Boundary Layer Integral Matrix Procedure (BLIMP) was selected by the JANNAF Boundary Layer Subcommittee as the standard performance evaluation method.

The primary purpose of this report is to present the results of a preliminary effort to provide a version of the BLIMP code that will serve as the standard boundary layer prediction tool for rocket nozzle flows. Section 2 contains a brief summary of the special modifications made to BLIMP to increase its utility to the rocket community. (Complete documentation of the original BLIMP code can be found in References 1 and 2.) The results of the verification tests for the four sets of data considered are contained in Section 3. In general the predictions are consistent with the data in the wall region of the boundary layer. This is based on wall heat flux comparisons. There are some discrepancies in the wake region; however, the predicted integral parameters are in reasonable agreement with the data. In one case, for a laminarizing turbulent flow, the heat flux predictions did not agree with the measurements. Section 4 contains recommendations for further code developments and improvements.

SECTION 2

CODE MODIFICATIONS

This section contains a brief discussion of the additions and modifications to the BLIMP code which have been incorporated as a result of the present work. Details of these modifications are contained in the interim user's manual, Reference 3. This new version of the BLIMP code has been denoted as version J to distinguish it from the standard BLIMP version.. Complete documentation of the original code is presented in References 1 and 2.

2.1 NAMELIST

The BLIMP code was modified to accept the nozzle wall contour as (x, R) coordinates in the namelist format output by the Two-Dimensional Kinetic (TDK) computer program (Reference 4). These coordinates are then used to calculate the nozzle wall length (assuming straight line segments between coordinate points) which is utilized in the internal coordinate system of the BLIMP code. The pressure ratio which is required by BLIMP is also in the TDK namelist. A subset (max 40) of the input stations (max 500) is then selected by the user to be the BLIMP solution stations.

2.2 THERMOCHEMICAL DATA

The BLIMP input format has been changed to accept the thermochemical constants for calculation of enthalpy, entropy, and specific heat in the polynomial form used by other JANNAF codes (Reference 5).

2.3 INPUT/OUTPUT CHANGES

In addition to the input changes described in Sections 2.1 and 2.2, the BLIMP code has been modified to accept input in either the International System of Units (SI) or the English Engineering System of Units. The entire output of the code has been formatted for SI units; however, in the case that English Units are used as input, they will also be used as output (the output headings remain in SI units). The output has also been modified to include the boundary layer thrust loss (ΔF), the total heat flux to wall (\dot{Q}_w), and the total wall area (A_w) calculated in the following manner:

$$\Delta F = 2\pi R \rho_e u_e^2 \theta \cos \phi \left(1 - \frac{P \delta^*}{\rho_e u_e^2 \theta}\right)$$

$$\dot{Q}_w = \int_0^s 2\pi R \dot{q} ds$$

$$A_w = \int_0^s 2\pi R ds$$

where s is the wall length and \dot{q} is the heat flux per unit area.

An option has been added to calculate a new body contour or a new inviscid flow field contour based on a correction to the input contour. The new contour is given by

$$R_{NEW} = R_{INPUT} \pm \delta^* \cos \phi$$

where the + sign is for a new body contour and the - sign is for a new inviscid flow contour. For example, if the input contour is the desired inviscid flow contour, then the new contour, calculated with the + sign, would be the corresponding nozzle wall contour. The new contour can be punched on cards in a form suitable for input to the TDK program.

2.4 REFIT OPTION

An option has been incorporated into the BLIMP code to adjust the nodal distribution as the solution moves downstream. This is accomplished by refitting the boundary layer profiles and shifting the nodes to insure that the nodes are always well placed. This option maintains a nodal distribution in the boundary layer which leads to better accuracy in defining the velocity profile and more efficient use of computation time.

SECTION 3

RESULTS OF VERIFICATION ANALYSIS

In a previous study (Reference 6) extensive comparisons of BLIMP predictions were made to experimental data. The cases considered included supersonic flow with zero pressure gradient, hypersonic flow with zero pressure gradient and with a favorable pressure gradient, hypersonic flow with nonreactive blowing, and supersonic flow with nonreactive blowing. Rather than repeat the broad range of cases considered in Reference 6, the present study focused only on rocket nozzle type flows, i.e., those flows with very large favorable pressure gradients. One case considered in Reference 6 (Brott et al., Reference 7) is of interest here and is discussed in Section 3.1.

New data sources were sought which would provide detailed and accurate velocity and temperature measurements in the boundary layer, skin friction measurements, or heat flux measurements in flows with pressure gradients of the same magnitude as those in rocket nozzles. The pressure gradient similarity is desired because it is expected to be the dominant term in the boundary layer equations. In addition, the data should contain stagnation and free stream pressure measurements, and stagnation and wall temperature measurements. The recent open literature was examined and members of the JANNAF Boundary Layer Subcommittee were requested to provide any data sets of which they had knowledge. Personal contacts at Rocketdyne and Aerojet were also requested to supply useful data on actual rocket firings.

The Rocketdyne data discussed in Section 3.2 is the only useful data which was found for actual liquid rocket engine tests. The input and some of the output for the predictions of this case are included in Reference 3 (the interim user's manual for this version of BLIMP) as a sample problem. The hot air space shuttle main engine (SSME) model test data were also supplied by Rocketdyne. These data consisted only of pitot tube measurements in the boundary layer at the exit of the nozzle; however, it was selected by NASA as a test case for BLIMP prediction. The most detailed, complete, and relevant data considered for verification was that of Back and Cuffel (Reference 8) and is discussed in Section 3.4. The input data and nozzle contours for the cases presented in Sections 3.2, 3.3, and 3.4 are contained in Appendix A.

No adjustments to the BLIMP code were attempted to obtain agreement between predictions and data. Modifications to the turbulent model and comparison with other models, e.g., Bushnell-Beckwith and Cebeci-Smith, should be investigated in future studies. Frequent reference is made to "the wall region" and "the wake region" of the boundary layer. In general these are rather loosely defined terms applied to turbulent boundary layers. The wall region refers approximately to the 10-20 percent of the boundary layer near the wall. This is the region in which the "law of the wall" part of the turbulent model in BLIMPJ is valid (see Reference 6 for a discussion of the turbulent model). The wake region is the remainder of the boundary layer.

3.1 DATA OF BROTT, YANTA, VOISINET, AND LEE

The hypersonic flow over a flat plate with favorable pressure gradient data of Brott, et al. (Reference 7) is most nearly representative of nozzle flows of the data considered in Reference 6; although, the pressure gradient is not nearly as severe (more than an order of magnitude difference). Representative comparisons from Reference 6 are shown in Figures 3-1 to 3-3 for stagnation conditions in air of

$$P_o = 1.013 \times 10^6 \text{ N/m}^2 \text{ (10 atm)}$$

$$T_o = 634.5^\circ\text{K} \text{ (610}^\circ\text{R)}$$

The momentum thickness Reynolds number ($Re_\theta = \rho_e u_e \theta / \mu_e$) comparison in Figure 3-2 provides information on the prediction of the overall boundary layer profile, since it is essentially an integral property. The skin friction coefficient ($C_{f/2} = \tau_w / \rho_e u_e^2$) comparison shown in Figure 3-3 is a measure of how well the velocity profile is predicted near the wall.

The conclusions from these three figures are that the predictions are very good at the wall (Figures 3-1 and 3-3) and that they are only slightly in error in the outer law of the wall region (Figures 3-1 and 3-2).

3.2 ROCKETDYNE: O_2/H_2 TWO-DIMENSIONAL NOZZLE

This case* is representative of the type of data that can be expected from hot fired nozzles using O_2/H_2 fuel systems. The gas side wall temperature and the wall heat flux distributions were measured; however, no boundary layer

* The data for this case were supplied by Mr. George Osugi of Rocketdyne.

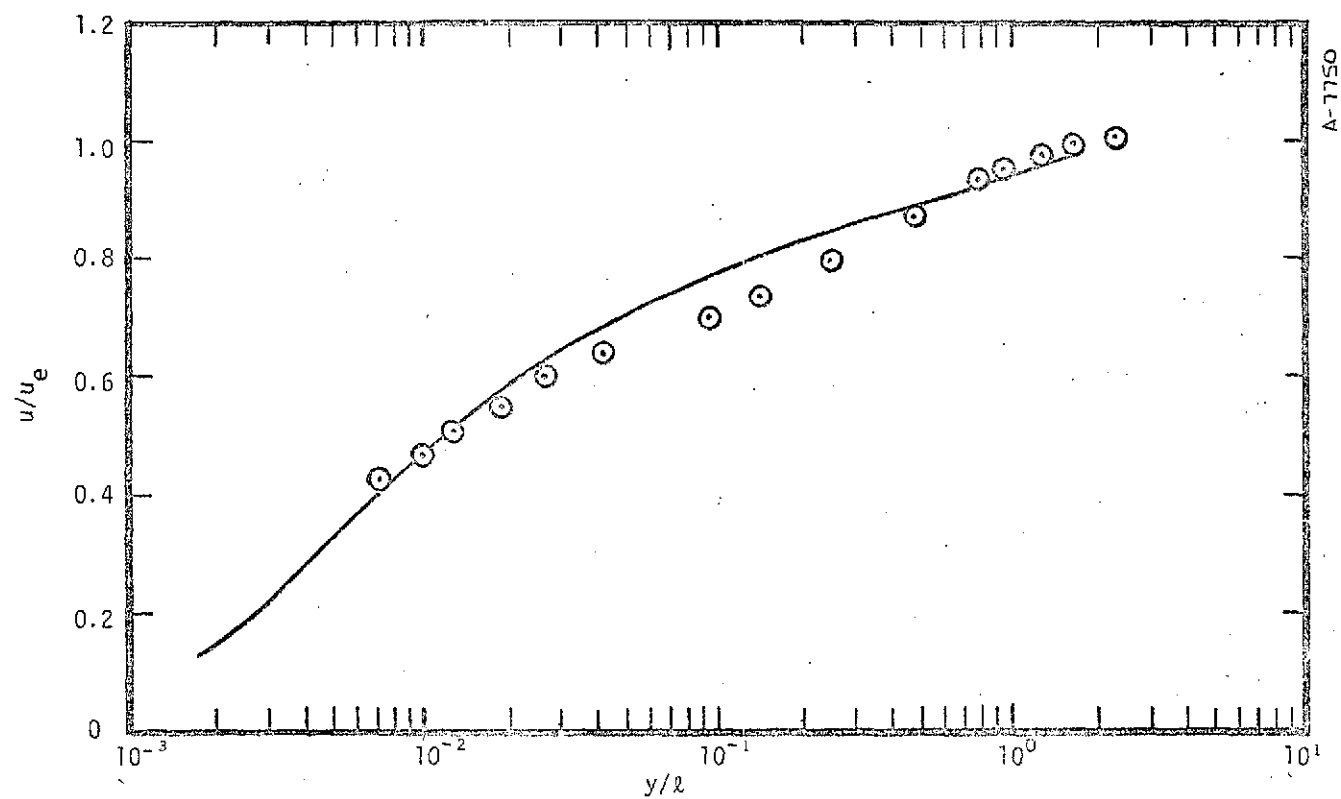


Figure 3-1. Linear-Log Velocity Profiles. Brott, et al.
 $X/L = 5.583$ ($L = 0.3048\text{m}$) [$l = .0254\text{m}$ (1 in)]
 ⊙ Brott's Data ($u_e = 825$ m/sec)
 — BLIMP Predictions ($u_e = 823$ m/sec)

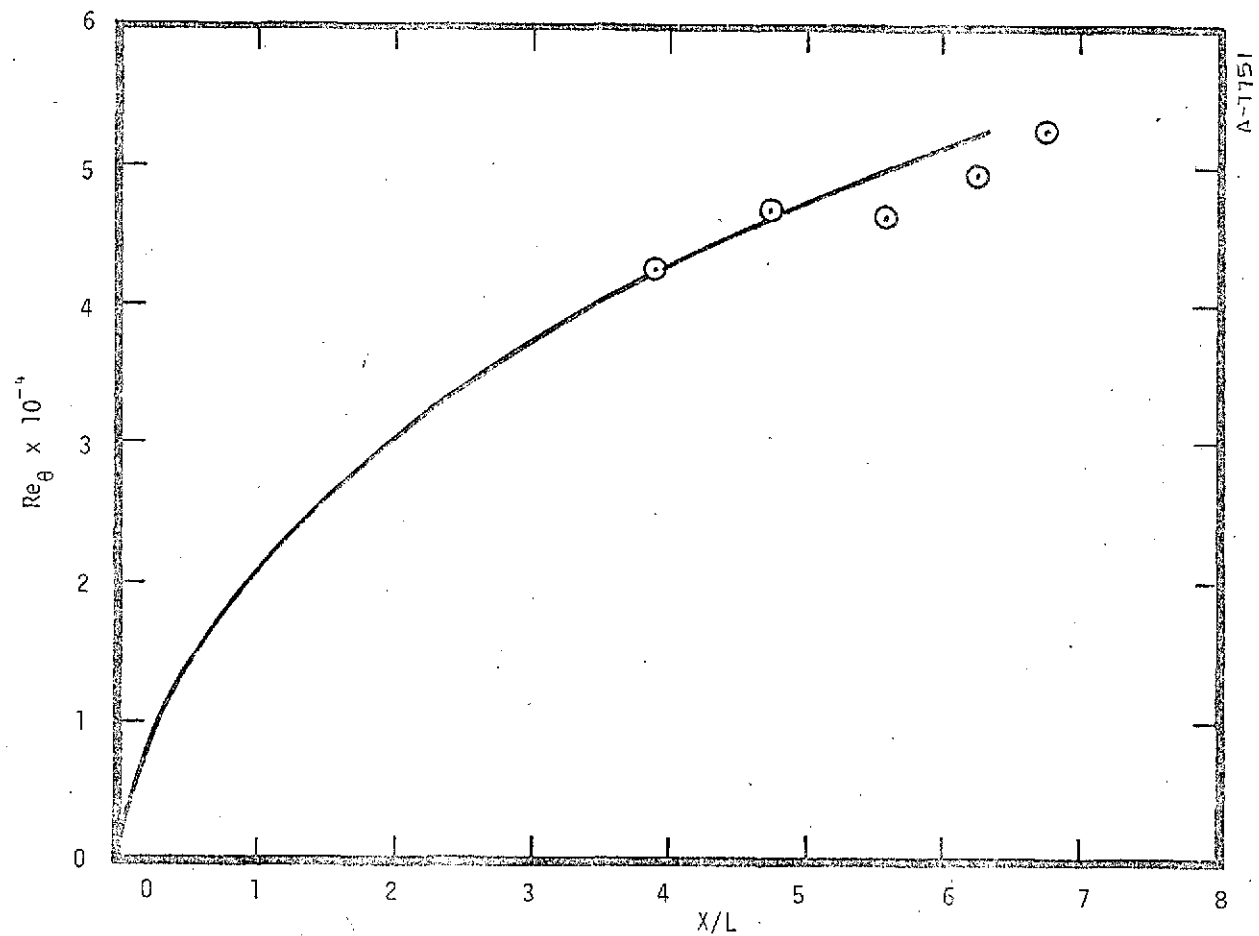


Figure 3-2. Momentum Thickness Reynolds Number. Brott, et al.

$L = 0.3048\text{m}(1 \text{ ft})$

○ Brott's Data
— BLIMP Prediction

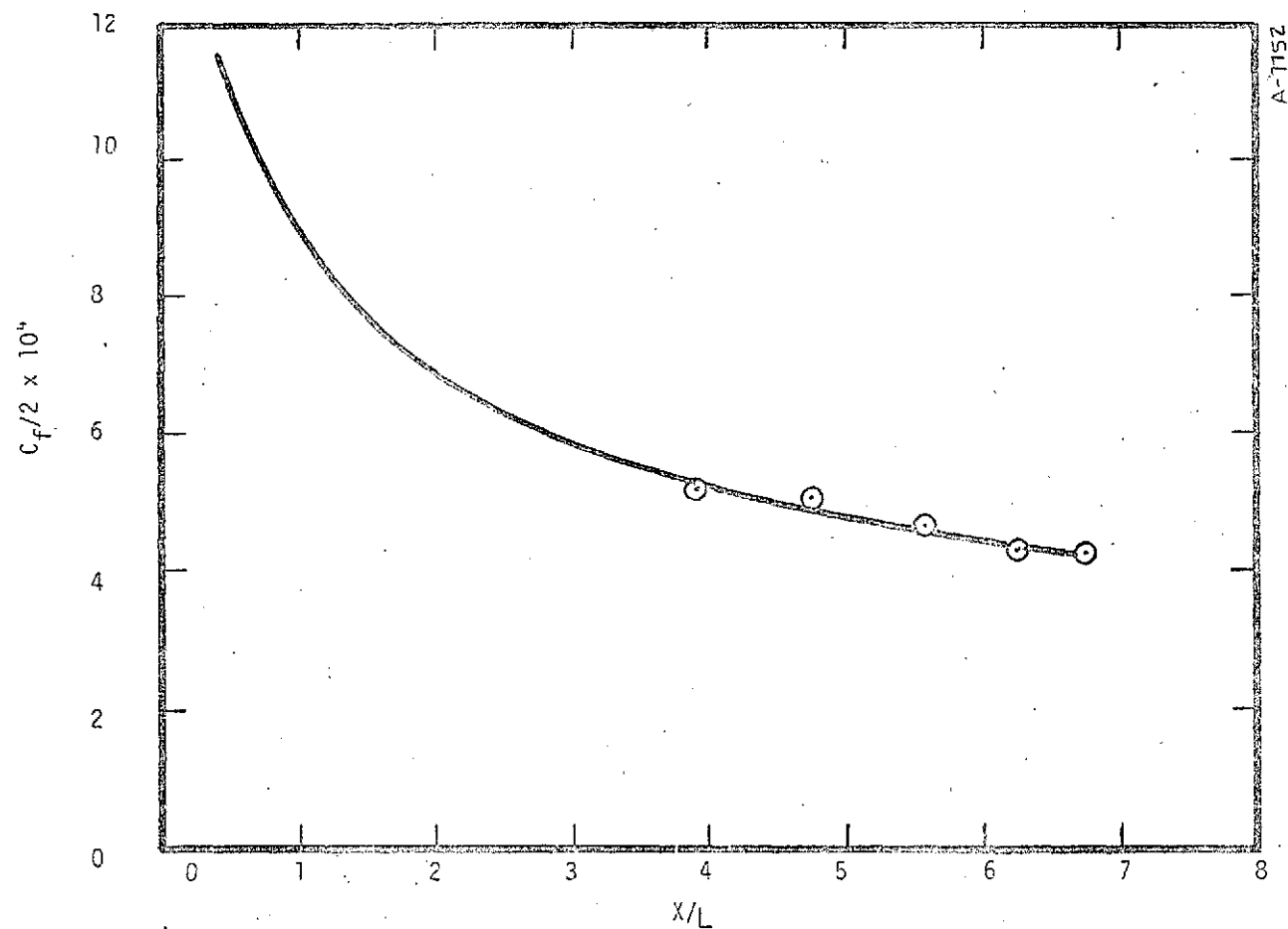


Figure 3-3. Skin Friction Coefficient. Brott, et al.

$L = 0.3048\text{m (1 ft)}$

○ Brott's Data
— BLIMP Solution

measurements were made. Since heat flux is an important quantity and this case was for a representative liquid rocket fuel it was felt that predictions would be of interest.

The nozzle geometry, fuel mixture ratio, stagnation conditions, calculated axial pressure variation, and wall temperature variation were provided. (The nozzle is .0762 m (3 in) wide.) The stagnation conditions were given as:

$$P_o = 4.6182 \times 10^6 \text{ N/m}^2 \text{ (45.57 atm)}$$

$$T_o = 3570^\circ\text{K (6430}^\circ\text{R)}$$

$$\text{M.R.} = 6.15$$

The injector plane was at the entrance to the nozzle and the initially low heat transfer shown by the data (Figure 3-4) was assumed to result from the presence of a liquid layer near the injector. Accordingly, the prediction was started downstream of the injector and assumed to have an established boundary layer at the starting position. The mixture ratio in the boundary layer was assumed to be 6.15. The heat flux data and the results of the BLIMP predictions are shown in Figure 3-4. The three cases shown in Figure 3-4 are for a fully turbulent boundary with a starting length of 0.0561 m, an initially laminar boundary layer with a starting length of 0.0561 m, and an initially laminar boundary layer with a starting length of 0.0286 m. (The starting length is the wall length from the start of the boundary layer growth to the first solution station. Adjustment of this length has the effect of changing the boundary layer thickness at the first solution station.) Transition for the laminar cases was at $Re_0 = 400$ and is shown on the figures. It is clear that the laminar boundary layers do not adequately predict the heat transfer. The turbulent predictions are approximately 60 percent too large near the throat. Thus it seems that the boundary layer should not be either laminar or turbulent, and the possibility of a laminarizing boundary layer should be investigated.

Schraub and Kline (Reference 9) have postulated that laminarization occurs in turbulent flows for values of the parameter $K = (v_e/u_e^2)(du_e/ds)$ exceeding about 3×10^{-6} (see also Reference 10). The value of K at the first solution station is 1.33×10^{-5} . This strongly suggests that the turbulent boundary layer is laminarizing, which would result in a reduction in heat flux. The value of K increases through the throat ($K_T = 2.81 \times 10^{-5}$) indicating that the flow would become even more "laminar like" in the throat region of the nozzle, thus reducing the heat flux from its turbulent value.

This test case leads to two very important conclusions. First, it is necessary to have reasonable knowledge of the nature of the history of the boundary

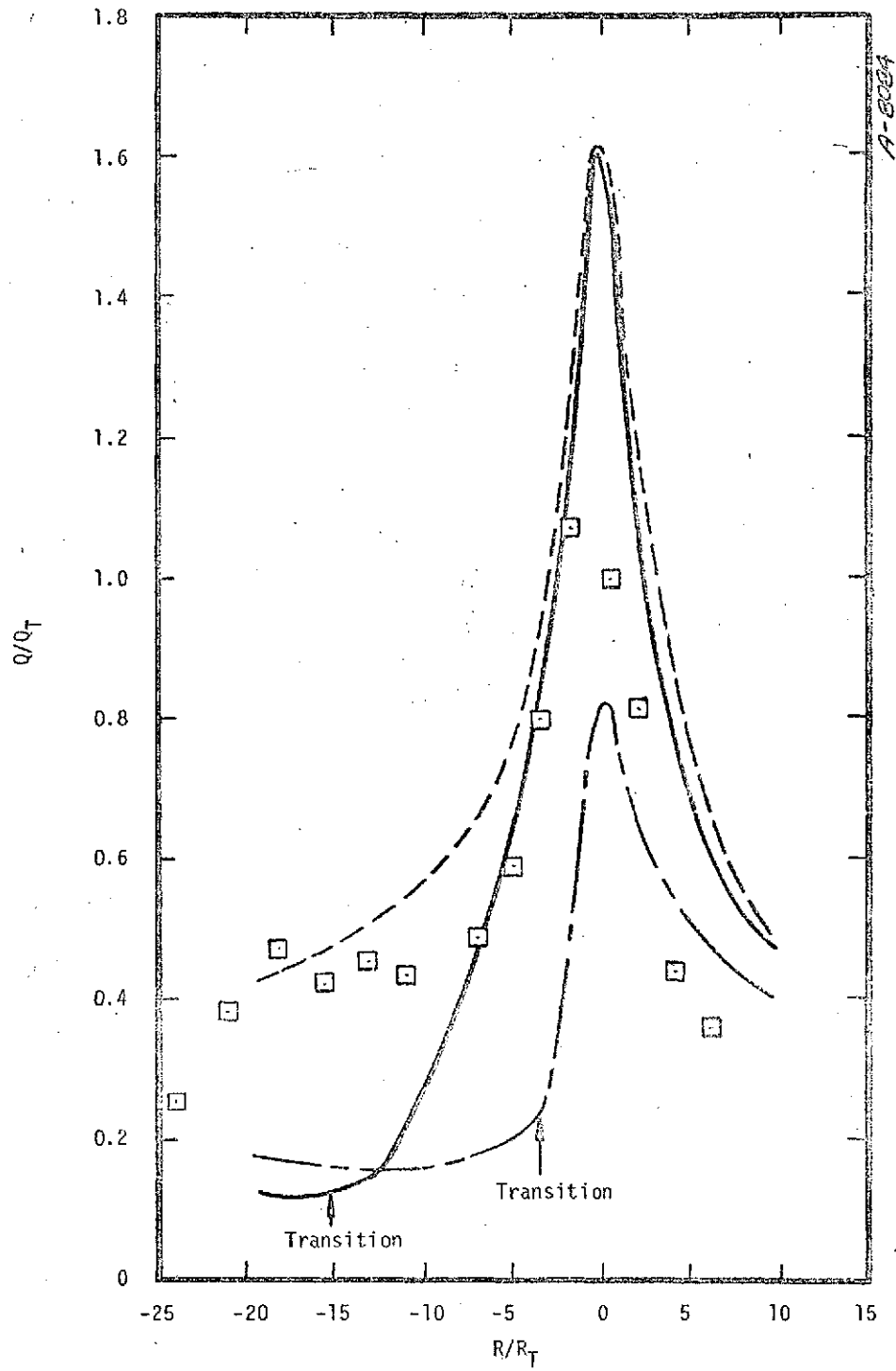


Figure 3-4. Comparison of Measured and Predicted Heat Flux for Rocketdyne O_2/H_2 Nozzle Flow

Throat radius: $R_T = 3.93 \times 10^{-3}$ m (0.155 in)

Q_T (the test value of heat flux at the throat) = 4.053×10^7 watts/m² (24.8 Btu/m²-sec)

□ Data

- BLIMP Predictions ($S_0 = 0.0561$ m, Transition $Re_0 = 400$)
- - - BLIMP Predictions ($S_0 = 0.0286$ m, Transition $Re_0 = 400$)
- - - BLIMP Predictions ($S_0 = 0.0561$ m, Fully Turbulent)

layer at the first solution station (e.g., did the boundary layer develop over a combustling liquid layer?). Secondly, laminarization of the rocket nozzle boundary layer may be a very significant effect and should be adequately modeled in the prediction tool.

3.3 SSME MODEL TEST - HOT AIR

These data from a heated air flow test in a 1:9.118 scale model of the space shuttle main engine were provided by Rocketdyne. Pitot tube measurements of the boundary layer were made in the exit plane of the nozzle (area ratio = 77.5). The pitot tube used in the wake region had dimensions 1.65×10^{-3} m O.D. (0.065 in) and 1.02×10^{-3} m I.D. (0.040 in). Near the wall the probe was flattened with O.D. of 3.04×10^{-4} m (0.012 in). The relationships of these probe sizes to the boundary layer dimensions are shown in Figure 3-5. Stagnation conditions were given as:

$$P_o = 1.027 \times 10^7 \text{ N/m}^2 \text{ (149 psia)}$$

$$T_o = 634.5^\circ\text{K} \text{ (610}^\circ\text{R)}$$

The wall contour was provided and, for the short duration of the test, the wall temperature was assumed constant at 294.4°K (530°R). The axial pressure distribution was provided from the output of the TDK program for the same conditions and geometry using the perfect gas option with ratio of specific heats = 1.4 and molecular weight = 28.58.

The results of the BLIMP predictions for boundary layer Mach number distribution at the exit plane are presented with the data in Figure 3-5. The Mach numbers were calculated from the measured pressures using normal shock relations. The major differences between the predictions and the data are in the region $0.05 < y/\delta < 0.37$. Two BLIMP predictions were made, one for transition at $Re_0 = 600$ and the other for fully turbulent flow. There was no significant difference in the results at the exit plane for the two cases. The predictions for the transition at $Re_0 = 600$ case are shown in all the figures. No laminarization effects are expected since the value of K at the throat is 4.83×10^{-7} .

The predicted momentum thickness and displacement thickness are shown in Figure 3-6. The agreement with the values calculated from the data is good; although, perhaps fortuitous. The predicted velocity profile and velocity profile calculated from the data are given in Figure 3-7. No temperature measurements were made in the boundary layer and all calculations from the data were

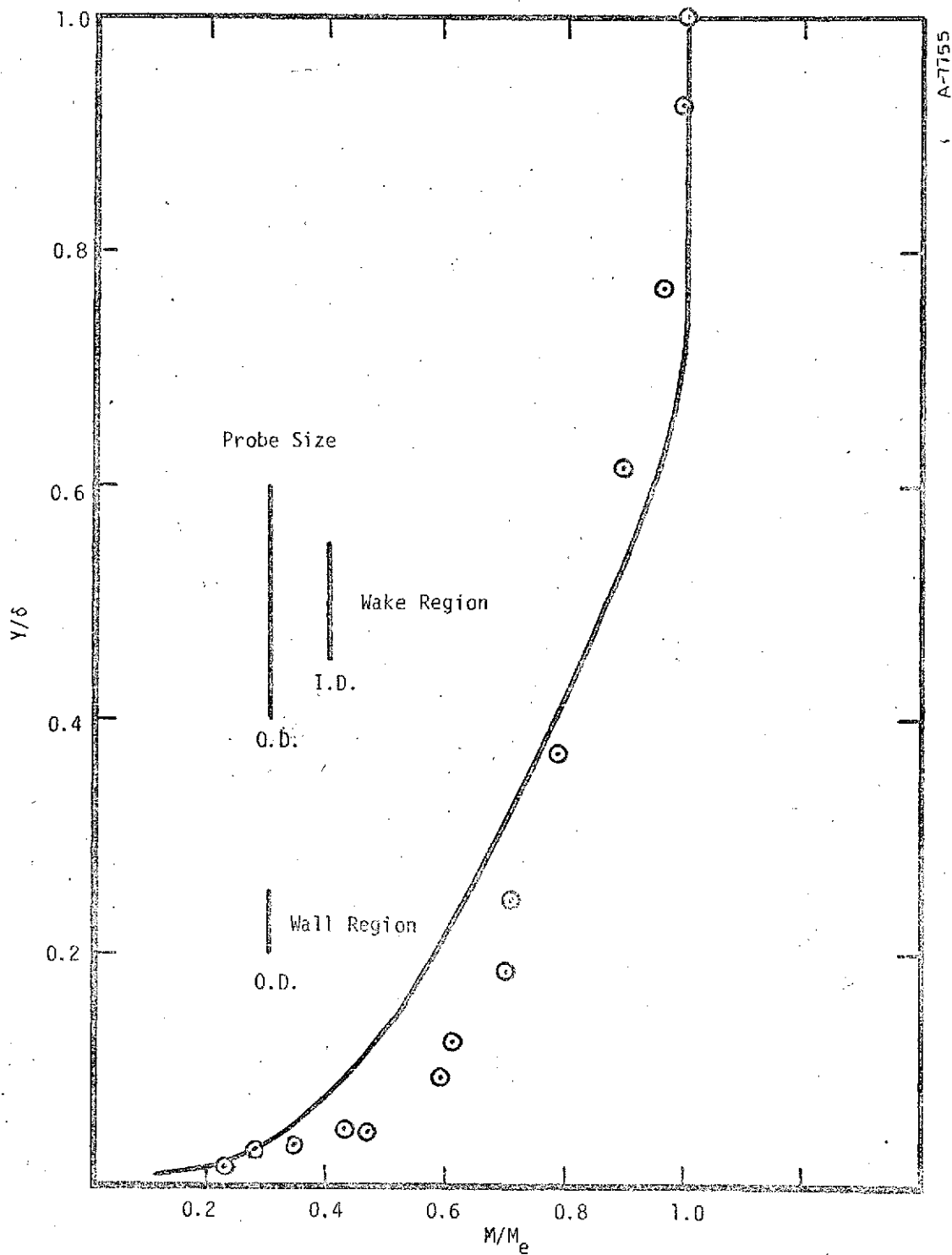


Figure 3-5. Comparison of Measured and Predicted Mach No. Profiles
SSME Model Test ($\epsilon = 77.5$)

$\delta = 0.008255$ m (0.325 in) (test value)

○ Rocketdyne Data (normalized by $M_e = 4.94$)

— BLIMP Predictions (normalized by $M_e = 5.18$)
(transition $Re_\theta = 600$)

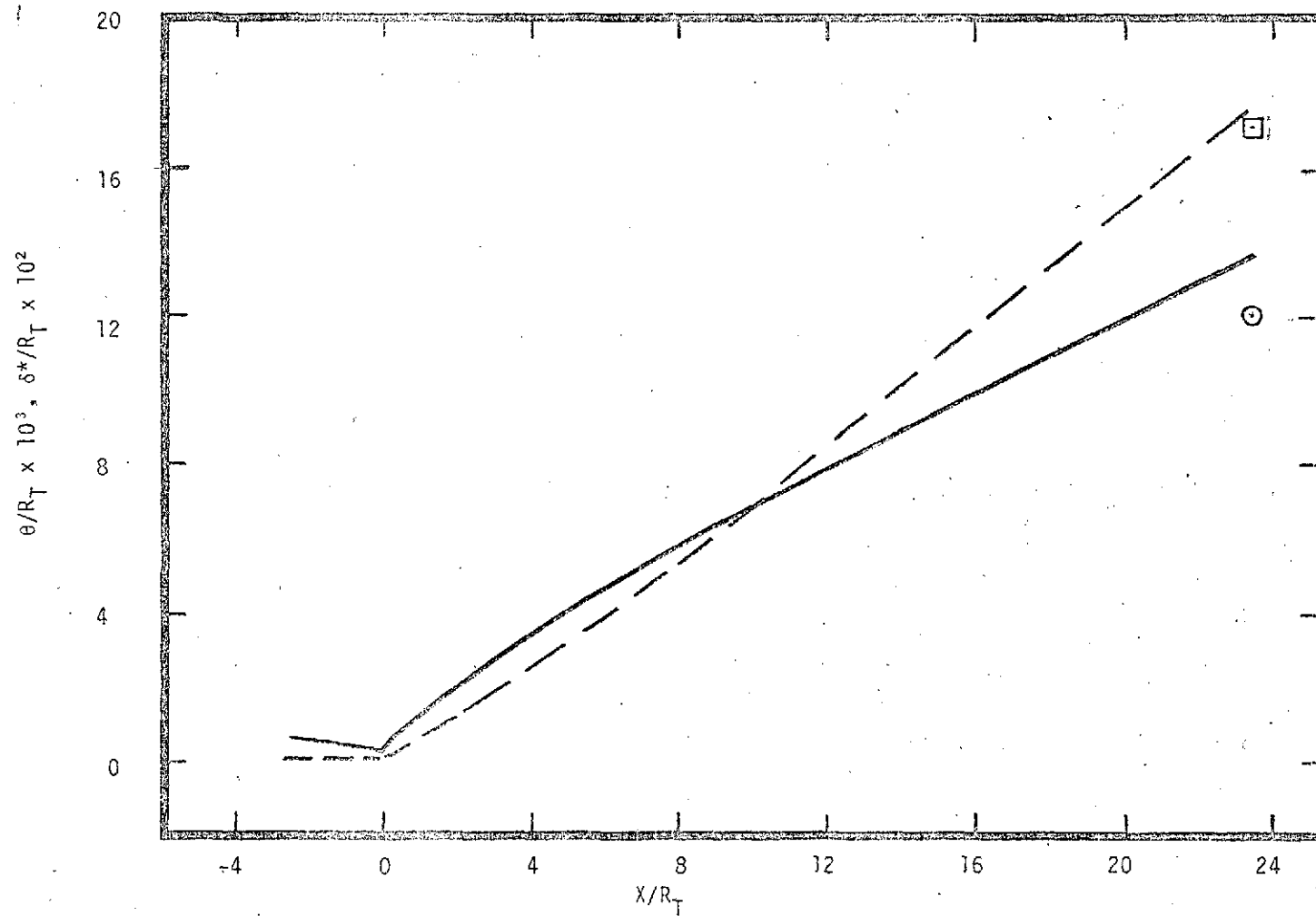


Figure 3-6. BLIMP Predictions for Momentum Thickness and Displacement Thickness
SSME Model Test

Throat radius: $R_T = 0.014351$ m (0.565 in)

— Momentum Thickness (○: test data result)
--- Displacement Thickness (□: test data result)

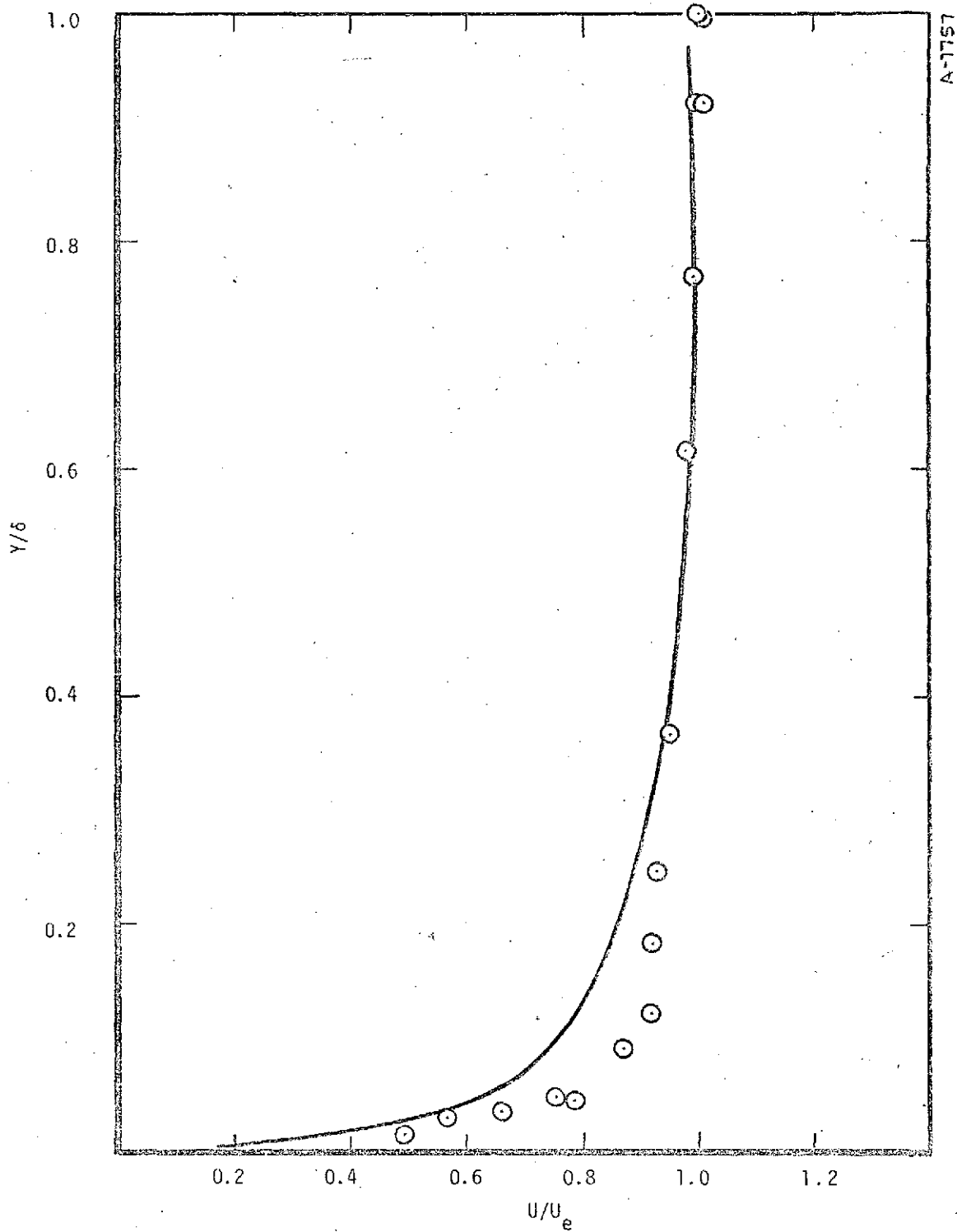


Figure 3-7. Comparison of Reported and Predicted Velocity Profile
 SSME Model Test ($\epsilon = 77.5$)
 $\delta = 0.008255$ m (0.325 in) (test value)
 ○ Rocketdyne Data (normalized by $u_e = 751$ m/sec)
 — BLIMP Prediction (normalized by $u_e = 763$ m/sec)

made by Rocketdyne assuming an adiabatic boundary layer.* Thus, calculated velocities would tend to be too large and this effect would increase as the wall is approached. This is reflected in Figure 3-7. The Mach number results are thus considered to be a more valid comparison.

Based on the fact that these predictions were made from completely analytical input, i.e., stagnation conditions and wall temperature, and pressure distribution calculated by the TDK program, the results are reasonably good. It should be pointed out that the BLIMP model for calculation of transport properties (μ and k) does not, in general, work well at very low temperatures such as those in the divergent region of this test case. In the present case, for example, the Prandtl number was calculated by the code to be 0.684 (one atmosphere, 273°K) as compared to a more reasonable value of 0.73. The overall effect of these discrepancies appears to be slight, particularly since much of the boundary layer is turbulent. It is recommended, however, that a homogeneous gas option with special low temperature properties for air be added to the code to predict room temperature air flows.

3.4 BACK AND CUFFEL -- SUPERSONIC NOZZLE WITH HEAT TRANSFER

These experiments were carried out in a cooled, conical nozzle with a convergent and a divergent half angle of 10° at the Jet Propulsion Laboratory, California Institute of Technology (Reference 8). The air flow was tripped well upstream of the converging section so that the flow was fully turbulent throughout the nozzle. These flow conditions are relevant to conditions in rocket engines operating at thrust levels for which laminarization does not occur and provide a good test for the basic BLIMP capabilities for rocket nozzle conditions. (The throat value for K , defined in Section 3.2, is 1.0×10^{-6} .)

Static pressures, wall heat fluxes, and coolant-side wall temperatures were measured along the nozzle wall. Heat flux was determined by calorimetric measurements in circumferential coolant passages. Boundary layer surveys were made with a flattened pitot probe 0.000127 m (0.005 in) in height and with thermocouple probes.

Velocity boundary layer profiles were measured at five stations; the locations of three of these are shown in Figure 3-8. The edge values of u_e for the predictions and the data are given in Table 3-1. In all the figures the test values of the various parameters are used as normalizing factors. The measured and predicted velocity profiles are shown in Figure 3-9 and the displacement thickness (δ^*) and momentum thickness θ , in Figure 3-10. The velocity profiles are in good agreement except for the position $X/R_T = -6.414$ where there

* Personal communications with Mr. Bill Wagner of Rocketdyne.

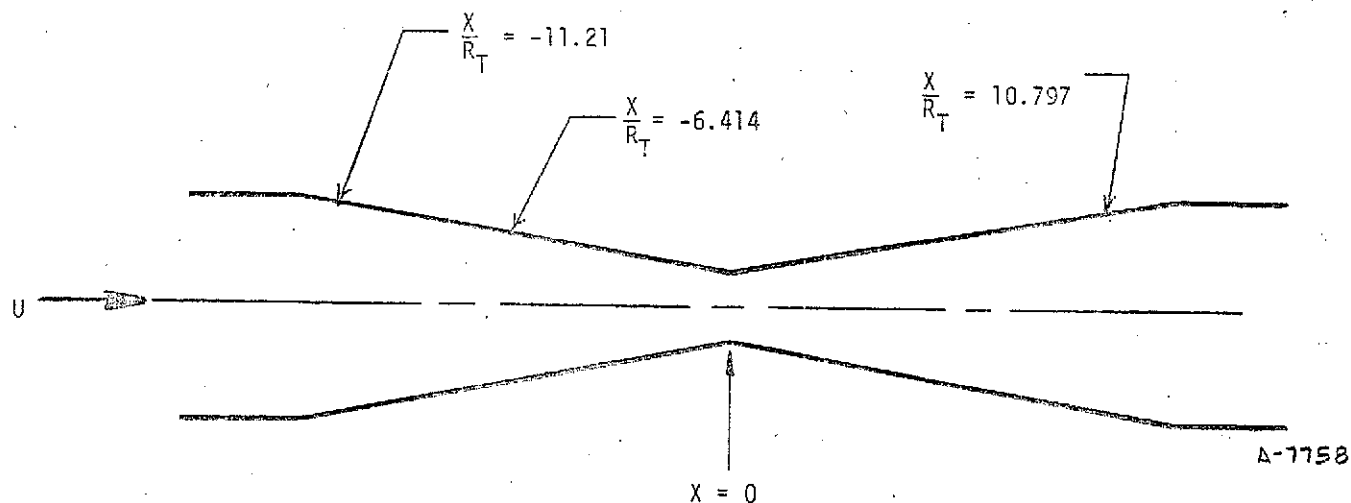


Figure 3-8. Schematic of Back and Cuffel Nozzle Showing Boundary Layer Probe Stations

$$R_T = 0.0202 \text{ m (0.795 in)}$$

$$\epsilon = 9.89$$

$$\text{Nozzle Length (Converging-Diverging Sections)} = 0.51 \text{ m (20.07 in)}$$

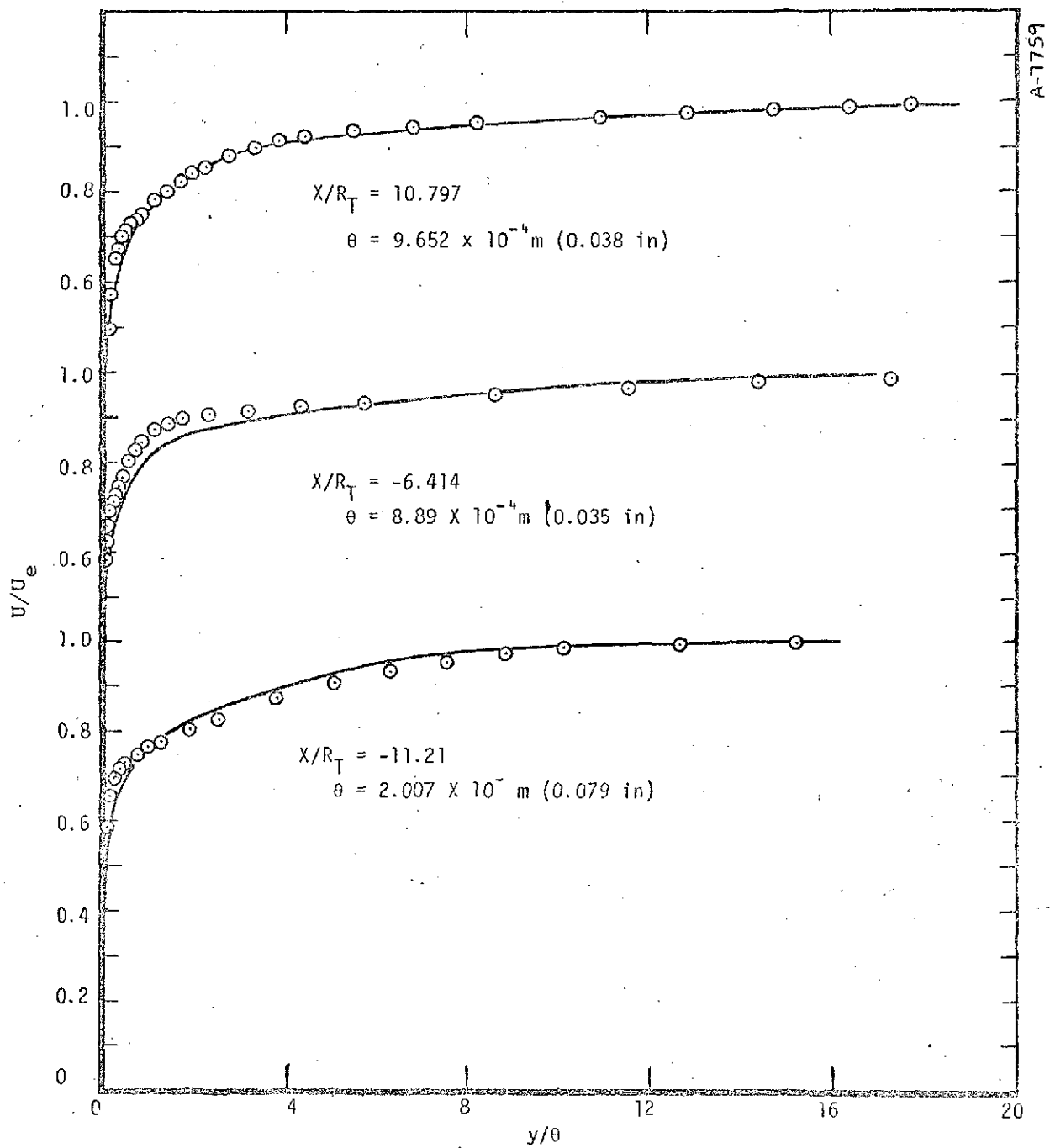


Figure 3-9. Measured and Predicted Velocity Boundary Layer Profiles For Back and Cuffel Data

(θ values are calculated from data)

(edge values of u_e are given in Table 3-1)

⊙ Data

— BLIMP Predictions

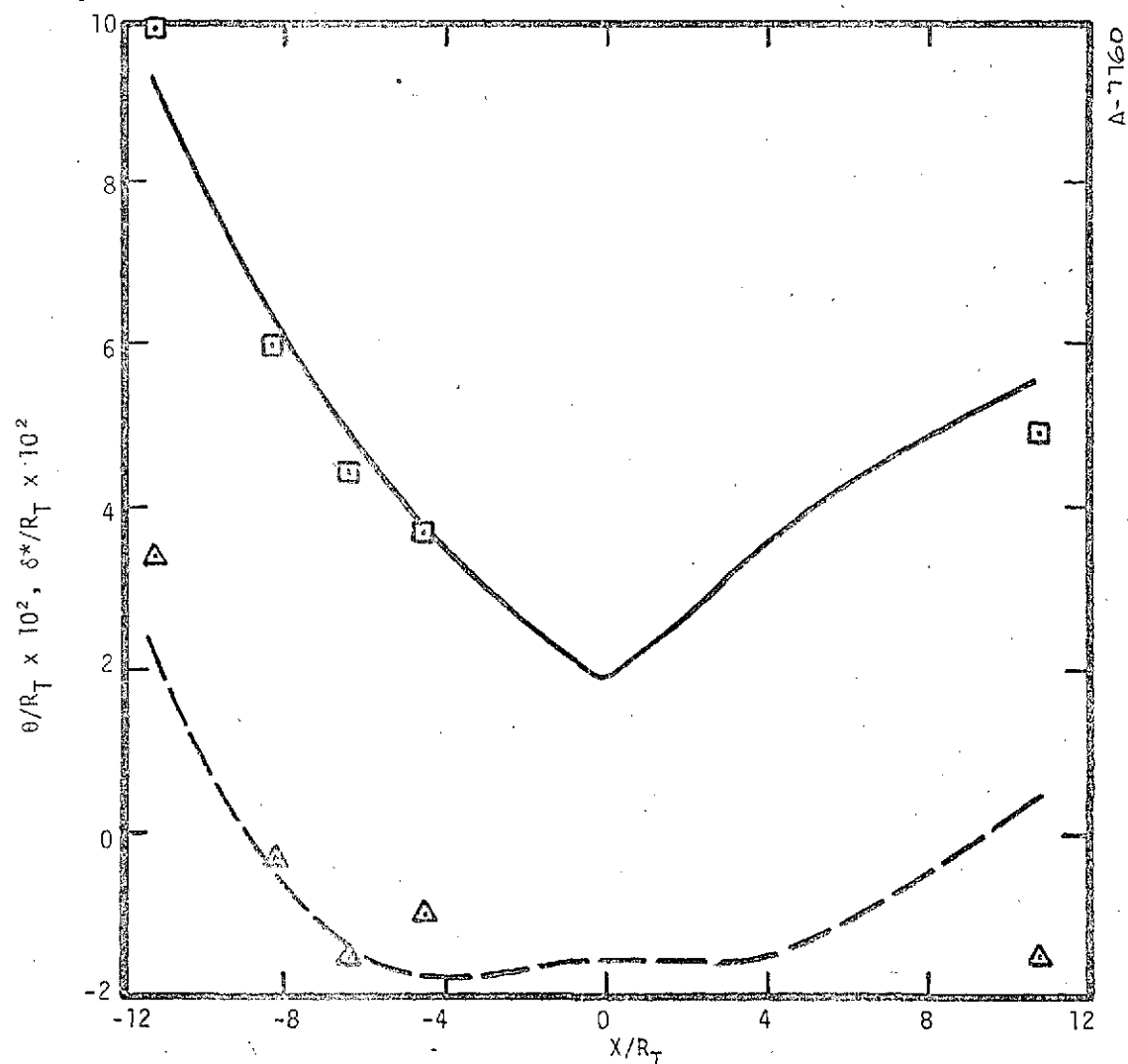


Figure 3-10. Momentum Thickness and Displacement Thickness For Back and Cuffel Data
Throat radius: $R_T = 0.0202\text{m}$ (0.795 in)

Δ - Data : δ^* Data : θ
 --- BLIMP Prediction: δ^* — BLIMP Predictions: θ

are differences (less than 10 percent, however) in the wake region. The integral properties θ and δ^* which reflect profile shape are in good agreement except at the position $X/R_T = 10.797$. The difference in δ^* is a consequence of a difference in the predicted and measured temperature profiles. The total temperature* profile is shown in Figure 3-11. (The normalizing factor is the value of $T_e^* - T_w^*$ from the data.) Since the velocity profiles at $X/R_T = 10.797$ are in very good agreement, the differences in total temperature can be attributed to differences in static temperature. These slight differences may result from the use of a constant value of 0.9 for the turbulent Prandtl number. The different shape of the static temperature profiles will cause different density profiles. The density-velocity product, mass flux, shown in Figure 3-12, is used for the calculation of δ^* . It is the large negative contribution to δ^* from the region above $\rho u / \rho_e u_e = 1$ in the data that causes the difference in the measured and predicted values of δ^* .

The near wall behavior can be evaluated by examining the heat flux data shown in Figure 3-13. The excellent agreement supports the conclusion that the near wall region is properly accounted for in BLIMP. The more detailed presentation of the velocity profile at $X/R_T = 10.797$ shown in Figure 3-14 shows that the data does not extend into the viscous sublayer region; therefore, one must rely on the heat transfer measurements for comparing wall behavior. The excellent overall agreement in velocity profiles is apparent.

TABLE 3-1

EDGE VALUES OF VELOCITY FOR BACK AND CUFFEL DATA

X/R_T	-11.21	-6.414	10.797
u_e (m/s), Data	42.0	79.4	1100.9
u_e (m/s), BLIMP	42.4	80.0	1111.6

3.5 SUMMARY

The two cases of Rocketdyne data represent almost completely analytical predictions, i.e., from given stagnation conditions and wall geometry an axial pressure variation was predicted and used in the boundary layer predictions. The two-dimensional nozzle predictions do not fit the data at all; however, the flow could well be of the laminarizing turbulent type for which the turbulent model in BLIMPJ has not been verified. Thus there is a need to investigate

Total temperature, T^ , is the measured stagnation temperature profile in the boundary layer.

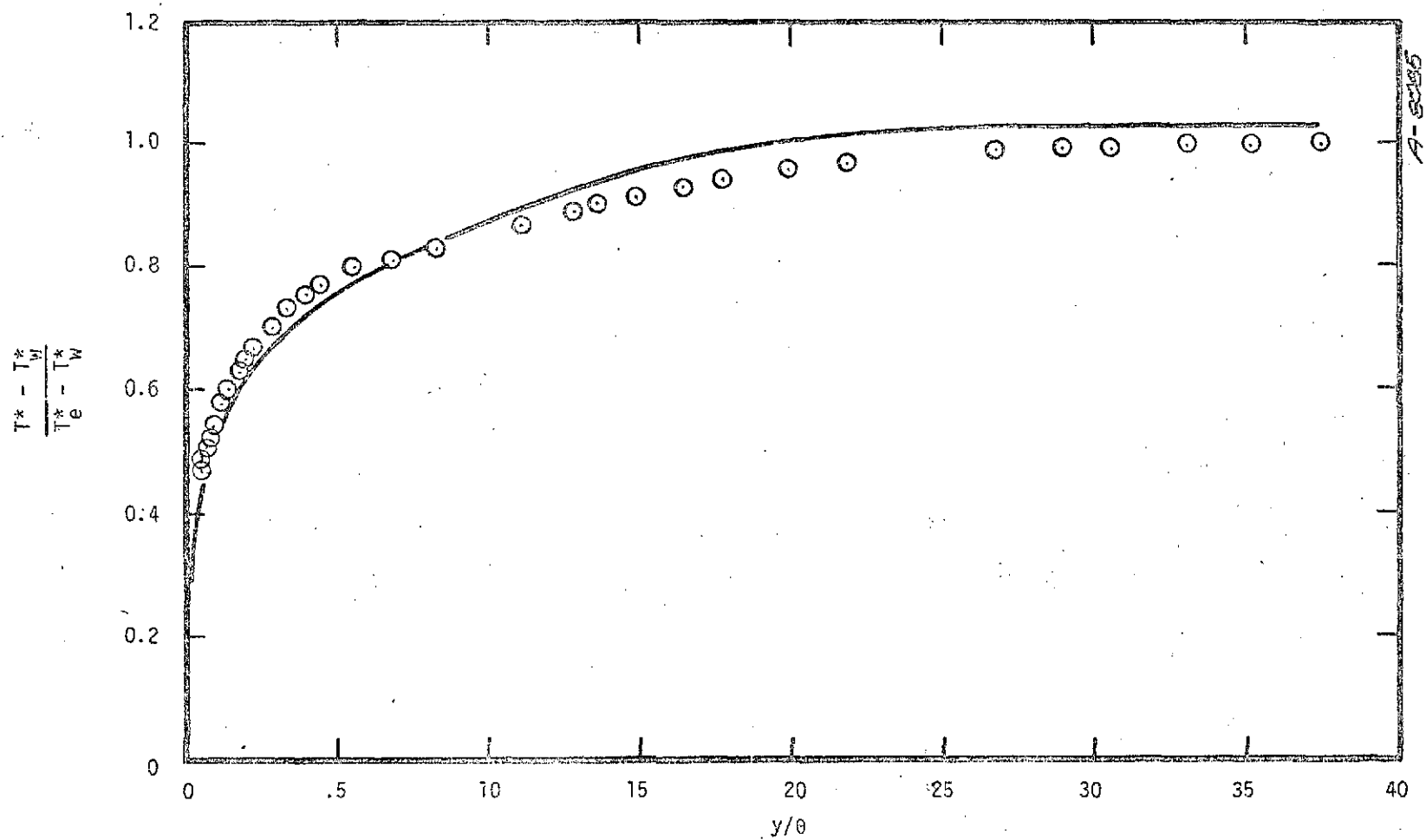


Figure 3-11. Measured and Predicted Total Temperature Profiles for
 Back and Cuffel Data, $X/R_T = 10.797$
 (θ calculated from data = $0.652 \times 10^{-4} \text{m}$)
 ○ Data ($T_e^* - T_w^* = 476^\circ\text{K}$, $T_w = 356^\circ\text{K}$)
 — BLIMP Predictions (normalized by 476°K , $T_e^* - T_w^* = 492^\circ\text{K}$, $T_w = 356^\circ\text{K}$)

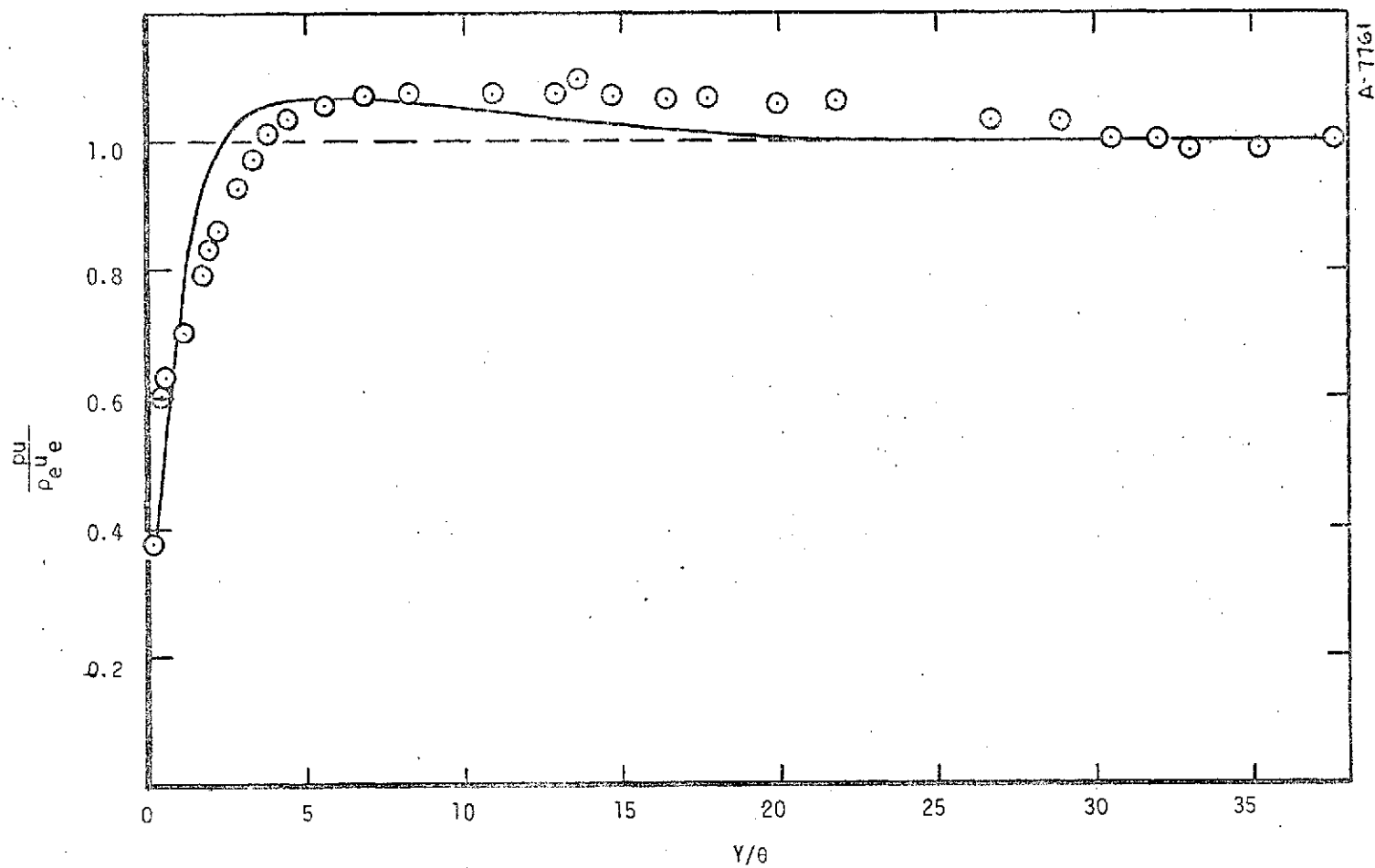


Figure 3-12. Comparison of Mass Flux Profile for Data of Back and Cuffel, $X/R_T = 10.797$

$\theta = 1.1176 \times 10^{-3} \text{ m (0.044 in)}$

⊙ Data ($\rho_e u_e = 201.3 \text{ kg/m}^2\text{-s}$)

— BLIMP Predictions ($\rho_e u_e = 198.5 \text{ kg/m}^2\text{-s}$)

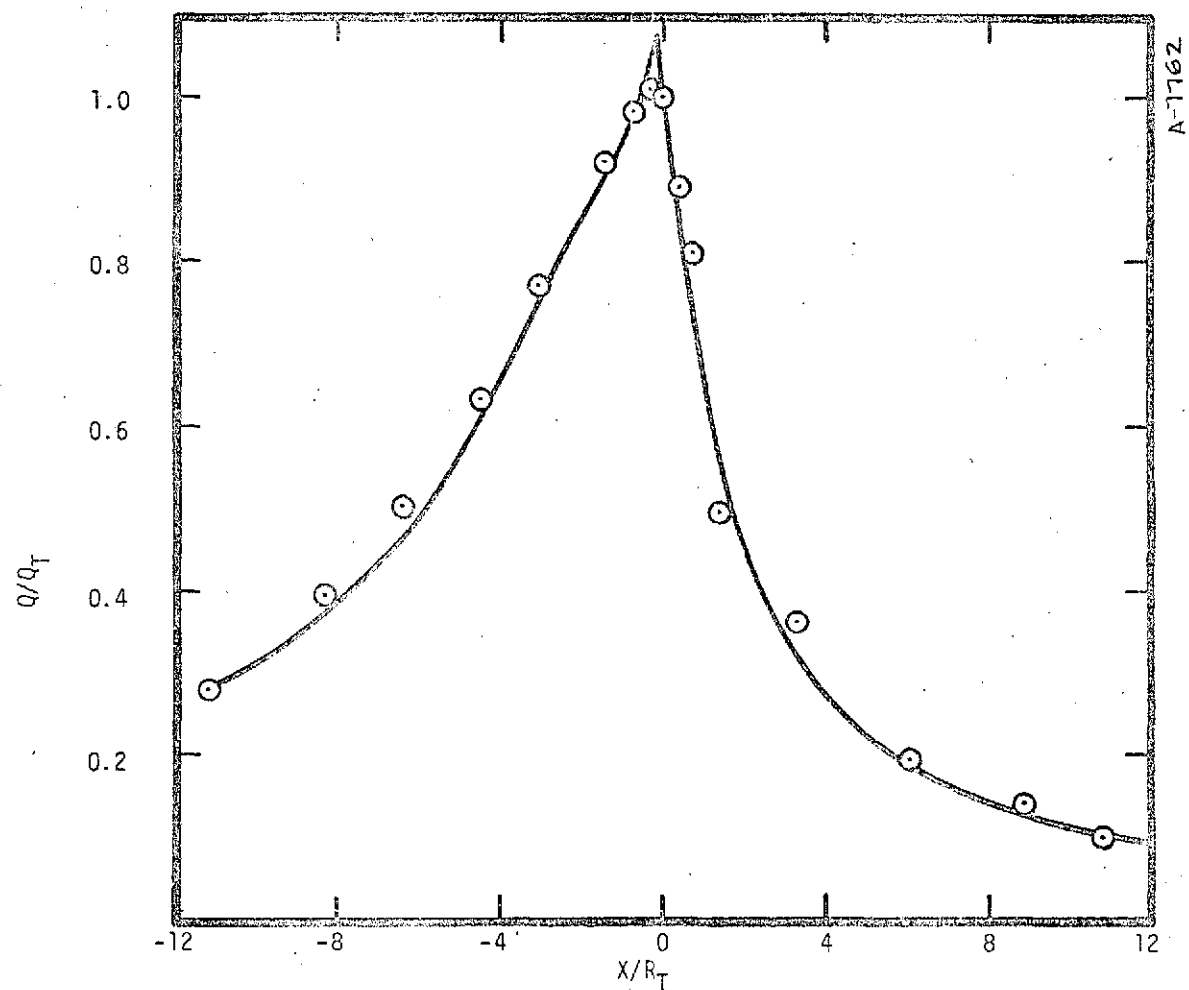


Figure 3-13. Comparison of Heat Flux Data and Predictions for Back and Cuffel Data; Heat Flux Measured At Throat: $Q_T = 547880 \text{ watts/m}^2$ ($.33538 \text{ Btu/in}^2\text{-sec}$)

○ Data

— BLIMP Predictions (Normalized to test value of Q_T)

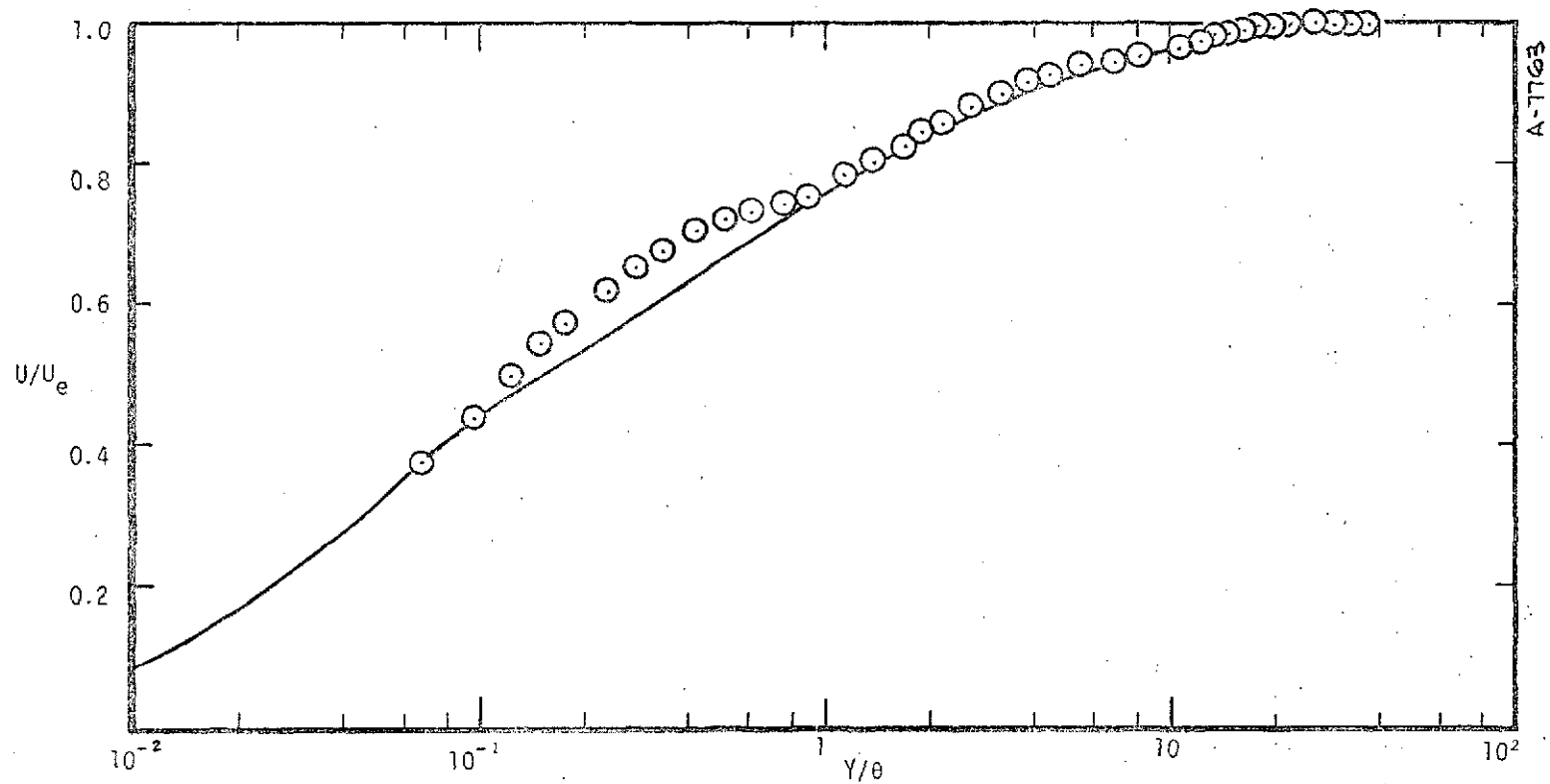


Figure 3-14. Comparison of Velocity Profile at $X/R_T = 10.797$ For Data of Back and Cuffel

$\theta = 9.652 \times 10^{-4} \text{ m (0.038 in) (test value)}$

○ Data ($u_e = 1100.9 \text{ m/s}$)

— BLIMP Predictions ($u_e = 1111.6 \text{ m/s}$)

the modeling of laminarization in the code. The SSME air flow data are reasonably well predicted. More detailed data of this type would be useful for code verification. In contrast, the data of Back (and of Brott) contained measured pressure distributions which were used as input to BLIMP. The resulting predictions show much better agreement with the data.

SECTION 4

RECOMMENDATIONS

As a result of working with BLIMP and rocket nozzle problems the following additions and modifications to the present version are suggested.

1. In order to provide the capability of comparison of results and potentially for the selection of the "better" model, the eddy viscosity models of Cebeci-Smith and Bushnell-Beckwith should be added to the code. Further verification of the present model (of Kendall) and comparison of the new models using experimental flows providing tests of various features of the models which are important to nozzle conditions should be made. Of particular interest is the prediction of laminarization.
2. Cold flow model tests using air, or other homogenous gases, could be treated by the BLIMP code without the use of the complete chemistry solution. Simplified procedures and improved computation economy could be achieved through the addition of a homogeneous gas option. This option could also offer the advantage of improved low temperature thermodynamic properties and transport properties.
3. For greater compatibility with the Two-Dimensional Kinetic program the following recommendations are made:
 - Addition of Kinetics
 - Improved matching of edge conditions on velocity, pressure, and their first derivatives, and improved curve fits of pressure gradient. The present method was not designed for the type of pressure distribution encountered in nozzle flow problems. For rocket nozzle flows the largest terms of the boundary layer momentum equation contain the gradient of pressure and the gradient of edge velocity; thus accuracy in these terms is most important.
4. The complexity of the input can be decreased by an expanded use of namelist input and built-in default values. This would greatly aid the inexperienced user and pose no limitations to the generality of the code.

5. Overall accuracy and computer usage could be improved by the following:

- Expanded three temperature range to provide for better low temperature curve fits of thermodynamic properties.
- Binary diffusion option for economy for problems with complex chemistry.
- Improved transport property calculations, especially for light elements and air.
- Improved built-in first guess of fully turbulent flows. The built-in first guess is for a laminar profile. For those problems with well-established turbulent profiles at the first solution station, a turbulent first guess would improve computer economy.
- Improved convergence criteria tailored to nozzle flows. The present convergence criteria have been developed and tested for reentry conditions where pressure gradients are not nearly so severe as in rocket nozzles.

REFERENCES

1. Anderson, L. W., E. P. Bartlett, and R. M. Kendall, "User's Manual, Boundary Layer Integral Matrix Procedure (BLIMP)," AFWL-TR-69-114, Vol. I, Air Force Weapons Laboratory, Kirtland AFB, New Mexico, March 1970.
2. Anderson, L. W. and R. M. Kendall, "User's Manual, Boundary Layer Integral Matrix Procedure (BLIMP)," AFWL-TR-69-114, Vol. II, Air Force Weapons Laboratory, Kirtland AFB, New Mexico, March 1970.
3. Evans, R. M. and H. L. Morse, "Interim User's Manual for Boundary Layer Integral Matrix Procedure, Version J," Acurex Corporation, Aerotherm Division, 1973.
4. Frey, H. M. and G. R. Nickerson, "Two-Dimensional Kinetic Reference Program," Dynamic Science, Irvine, California, December 1970.
5. McBride, B. J. and S. Gordon, "Fortran IV Program for Calculation of Thermodynamic Data," NASA-TN-D-4097, Lewis Research Center, Cleveland, Ohio, August 1967.
6. Anderson, L. W. and H. L. Morse, "A Turbulent Model Study for the Multi-component Nonsimilar Turbulent Boundary Layer Program," Air Force Weapons Laboratory, Kirtland Air Force Base, New Mexico, AFWL-TR-71-57, October 1971.
7. Brott, D. L., W. J. Yanta, R. L. Voisinnet, and R. E. Lee, "An Experimental Investigation of the Compressible Turbulent Boundary Layer With a Favorable Pressure Gradient," NOLTR-69-143, U. S. Naval Ordnance Laboratory, White Oak, Maryland, August 1969.
8. Back, L. H. and R. F. Cuffel, "Turbulent Boundary Layer and Heat Transfer Measurements Along a Convergent-Divergent Nozzle," Journal of Heat Transfer, November 1971, p. 397-407.
9. Shraub, F. A. and S. J. Kline, "A Study of the Structure of the Turbulent Boundary Layer With and Without Longitudinal Pressure Gradients," Report No. MD-12, Department of Mechanical Engineering, Stanford University, March 1965.
10. Back, L. H., R. F. Cuffel, and P. F. Massier, "Laminarization of a Turbulent Boundary Layer in Nozzle Flow - Boundary Layer and Heat Transfer Measurements With Wall Cooling," Journal of Heat Transfer, Trans. ASME, Series C, Vol. 92, No. 3, August 1970.

APPENDIX A

INPUT DATA AND NOZZLE CONTOURS

A.1 ROCKETDYNE O₂/H₂ TWO-DIMENSIONAL NOZZLE INPUT DATA

```

10100321210202000000 TEST CASE ROCKETDYNE - PUNCH - R-DELTA*CD3      01100 A
2.                                                                    02100 A
19                                                                    03100 A
14.25                                                                    03201 A
49 30                                                                    03300 A
9 12 16 19 21 23 25 27 29 31 32 33 35 39 03401 A
41 44 46 47 49 03402 A

SYNPUT
XITAB= 0.0 0.0 0.0 -25.806 -24.516 -23.226 -21.935
-19.645 -18.355 -16.064 -16.774 -15.484 -14.193 -12.903
-11.600 -10.322 -8.645 -7.742 -6.452 -5.161 -3.871 -2.181
-1.935 -1.613 -1.290 -0.968 -0.545 -0.323 -0.194 0.0
0.0181 0.1303 0.2832 0.4271 0.5639 0.7226 0.880 1.032
1.1232 1.390 1.553 2.015 3.007 4.024 5.007 6.724
5.942 10.720 11.975 YITAB= 0.0 0.0 0.0 6.548
6.387 6.219 6.345 5.864 5.671 5.471 5.264 5.039
4.807 4.561 4.297 4.019 3.716 3.387 3.032 2.632
2.187 1.484 1.374 1.258 1.161 1.090 1.062 1.013
1.006 1.000 1.0001 1.0019 1.0077 1.0174 1.0310 1.0510
1.0761 1.1039 1.1239 1.1903 1.2342 1.3858 1.6239 1.8961
2.160 2.938 3.217 3.690 4.000 PITAB= 0.0 0.0
0.0 0.9953 0.9951 0.0 0.9944 0.0 0.9934 0.0
0.0 0.9918 0.0 0.0 0.0 0.9876 0.0 0.0
0.9771 0.0 0.9565 0.0 0.8734 0.0 0.7806 0.0
0.6653 0.0 0.577 0.0 0.531 0.5071 0.4774 0.0
0.4151 0.0 0.0 0.3204 0.0 0.0 0.2554 0.0
0.0 0.1446 0.0 0.0750 0.0609 0.0 0.0474

SEND
12 0.002 0.006 0.01 0.025 0.06 0.15 04100 A
0.0 0.002 0.006 0.01 0.025 0.06 0.15 04201 A
0.4 0.7 1.0 1.5 2.5 0.06 0.15 04202 A
10.0 95 1 3.0 5 0.12 0.25 0.35 0.45 0.6 04300 A
0.0 0.05 0.12 0.25 0.35 0.45 0.6 04401 A
0.15 0.85 0.95 0.98 1.0 0.05 0.6 04402 A
0.03937 05100 A
4.6182E+06 07100 A
9.0748E+04 07200 A
07300 A
08100 A
-12.18E+06 09600 A
2. 11100 A
H HYDROGEN 1.008 -1.0 11201 A
O OXYGEN 16.0 -6.15 11202 A
300. 1000. 5000. 13100 A
H J 9/65H 1. G 300. 5000.
0.25 E+01 0. 0. 0. 0.
0.25471620E+05=0.46011763E+00 0.25 E+01 0. 0.
0. 0. 0.25471627E+05=0.46011762E+00
0. J 6/620 1. G 300. 5000.
0.25420596E+01=0.27550619E-04=0.31028033E+08 0.45510674E-11=0.43680515E-15
0.29230803E+05 0.49203080E+01 0.29464287E+01=0.15381665E-02=0.24210316E-05
=0.16028432E+08 0.38906964E-12 0.29147644E+05 0.29639949E+01
02. J 9.650 2. G 300. 5000.
0.36219535E+01 0.73618264E-03=0.19652228E-06 0.36201558E-10=0.28945627E-14
=0.12019825E+04 0.36150960E+01 0.36255905E+01=0.18782184E-02 0.70554544E-05
=0.67635137E+08 0.21555993E-11=0.10475226E+04 0.43052778E+01
H2. J 3/61H 2. G 300. 5000.
0.31001901E+01 0.51119464E-03 0.52644210E-07=0.34909973E-10 0.36945345E-14
=0.87733042E+03=0.19629421E+01 0.30574451E+01 0.26765200E-02=0.58099162E-05
0.55210391E+08=0.18122737E-11=0.78890474E+03=0.22997056E+01
OK. J 3/66D 1. H 1. G 300. 5000.
0.29106427E+01 0.95931650E-03=0.19441702E-06 0.13756646E-10 0.14224542E-15
0.39353815E+04 0.54423445E+01 0.36375943E+01=0.10778858E-02 0.96830378E-06
0.18713972E-09=0.22571094E-12 0.36412823E+04 0.49370009E+00

```

H2O J 3/61H 2, 0 1, G 300, 5000, 1
 0,27167633E+01 0,29451374E+02 0,80224374E+06 0,10226682E+09 0,48472145E+14 2
 0,29905826E+05 0,66305671E+01 0,40701275E+01 0,11084499E+02 0,41521130E+05 3
 0,29637404E+08 0,80702103E+12 0,30279722E+05 0,32270046E+00 4
 13LAST A
 15201 A
 15202 A
 15203 A
 16201 A
 16202 A
 16203 A
 16601 A
 16602 A
 16603 A
 16604 A
 16605 A
 16606 A
 16607 A
 16608 A
 16609 A
 LAST A

630,	650,	658,	700,	861,	919,	911,
906,	900,	894,	888,9	886,	883,	869,
833,	708,	544,	488,	422,		

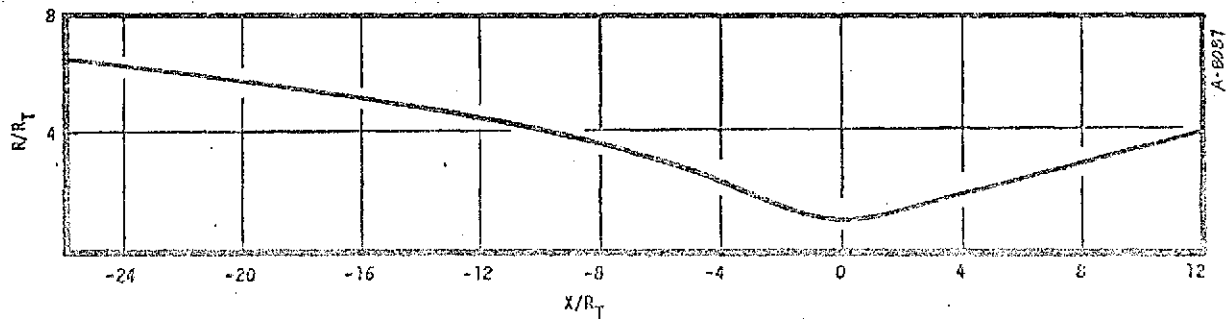


Figure A-1. Rocketdyne 2-D Nozzle Contour

Area Ratio = 4.0
 Aspect Ratio (Width/ R_T) = 22.8
 Length = 0.1484 m (5.846 in)
 R_T = 0.003937 m (0.155 in)

A.2 SSME MODEL TEST

```

1. 10500620210202000000 SSME -HOT AIR TEST SCALE=9.118 LAM/TURB TRANS 01100 A
2. 2 02100 A
3. 27 03100 A
4. 0.24 03201 A
5. 348 14 03300 A
6. 12 3 6 8 10 11 12 13 14 20 39 42 43 44 03402 A
7. 46 48 57 66 87 122 181 264 299 320 334 345 348 03402 A
8. INPUT
9. XITAB(1)= -2.717022, -2.47788, -2.15826, -2.010015, -1.565286, -1.194646,
10. -.9722726, -.8240237, -.527525, -.3792768, -.2310278, -.11589032, -.0337625,
11. 0.000000, 6.075117-03, 1.231079-02, 1.276280-02, 2.525359-02,
12. 3.194245-02, 3.877306-02, 4.574314-02, 5.285351-02, 6.010457-02, 6.749546-02,
13. 7.502766-02, 8.270299-02, 9.052509-02, 9.849772-02, 1.066222-01, 1.149025-01,
14. 1.233485-01, 1.319600-01, 1.407471-01, 1.497183-01, 1.588726-01, 1.682407-01,
15. 1.778118-01, 1.876086-01, 1.976402-01, 2.079257-01, 2.184800-01, 2.293244-01,
16. 2.406556-01, 2.520149-01, 2.632081-01, 2.744028-01, 2.856230-01, 2.968561-01,
17. 3.081009-01, 3.193750-01, 3.306298-01, 3.419418-01, 3.532205-01, 3.645818-01,
18. 3.759130-01, 3.872946-01, 3.987101-01, 4.101256-01, 4.216062-01, 4.330668-01,
19. 4.445857-01, 4.561464-01, 4.677053-01, 4.793492-01, 4.909567-01, 5.026377-01,
20. 5.143794-01, 5.260996-01, 5.378936-01, 5.497450-01, 5.615861-01, 5.735022-01,
21. 5.854734-01, 5.974463-01, 6.094928-01, 6.215946-01, 6.337071-01, 6.458950-01,
22. 6.581369-01, 6.703973-01, 6.827351-01, 6.951290-01, 7.075445-01, 7.200408-01,
23. 7.325961-01, 7.451761-01, 7.578391-01, 7.719990-01, 7.861871-01, 8.004986-01,
24. 8.148028-01, 8.292338-01, 8.437684-01, 8.583116-01, 8.729813-01, 8.877509-01,
25. 9.025464-01, 9.174677-01, 9.324844-01, 9.475442-01, 9.627294-01, 9.780056-01,
26. 9.933420-01, 1.008842+00, 1.024326+00, 1.039969+00, 1.055752+00, 1.071532+00,
27. 1.087473+00, 1.103549+00, 1.119638+00, 1.135388+00, 1.152272+00, 1.168681+00,
28. 1.185253+00, 1.201958+00, 1.218703+00, 1.235611+00, 1.252649+00, 1.269742+00,
29. 1.287000+00, 1.304583+00, 1.321839+00, 1.339461+00, 1.357202+00, 1.375037+00,
30. 1.393036+00, 1.411149+00, 1.429378+00, 1.447812+00, 1.466244+00, 1.483150+00,
31. 1.498510+00, 1.513937+00, 1.529394+00, 1.544957+00, 1.560619+00, 1.576256+00,
32. 1.592015+00, 1.607863+00, 1.623774+00, 1.639720+00, 1.655781+00, 1.671950+00,
33. 1.688087+00, 1.704369+00, 1.720742+00, 1.737184+00, 1.753664+00, 1.770269+00,
34. 1.786990+00, 1.803678+00, 1.820524+00, 1.837467+00, 1.854484+00, 1.871546+00,
35. 1.888741+00, 1.906058+00, 1.923344+00, 1.940798+00, 1.958426+00, 1.975943+00,
36. 1.993663+00, 2.011490+00, 2.029445+00, 2.047374+00, 2.065478+00, 2.083762+00,
37. 2.101940+00, 2.120320+00, 2.138832+00, 2.157460+00, 2.176077+00, 2.194875+00,
38. 2.213852+00, 2.232733+00, 2.251832+00, 2.271052+00, 2.290387+00, 2.309738+00,
39. 2.329268+00, 2.348966+00, 2.368596+00, 2.388443+00, 2.408418+00, 2.428486+00,
40. 2.448613+00, 2.468912+00, 2.489357+00, 2.509779+00, 2.530409+00, 2.551237+00,
41. 2.571960+00, 2.592926+00, 2.614028+00, 2.635239+00, 2.656494+00, 2.677940+00,
42. 2.699544+00, 2.721115+00, 2.742907+00, 2.764911+00, 2.786802+00, 2.808946+00,
43. 2.831237+00, 2.853629+00, 2.876083+00, 2.898732+00, 2.921528+00, 2.944316+00,
44. 2.967325+00, 2.990531+00, 3.013656+00, 3.037030+00, 3.060650+00, 3.084117+00,
45. 3.107860+00, 3.131760+00, 3.155762+00, 3.179930+00, 3.204101+00, 3.228517+00,
46. 3.252940+00, 3.277587+00, 3.302420+00, 3.327201+00, 3.352227+00, 3.377480+00,
47. 3.402627+00, 3.428038+00, 3.453714+00, 3.479239+00, 3.505038+00, 3.531009+00,
48. 3.557065+00, 3.583232+00, 3.609605+00, 3.636100+00, 3.662683+00, 3.689491+00,
49. 3.716483+00, 3.741157+00, 3.766843+00, 3.793827+00, 3.941865+00, 4.000961+00,
50. 4.061393+00, 4.122955+00, 4.185528+00, 4.249462+00, 4.314761+00, 4.381145+00,
51. 4.448709+00, 4.517682+00, 4.588077+00, 4.659587+00, 4.732327+00, 4.806527+00,
52. 4.882204+00, 4.959178+00, 5.037312+00, 5.116979+00, 5.198201+00, 5.281012+00,
53. 5.365444+00, 5.451202+00, 5.538635+00, 5.627842+00, 5.718910+00, 5.811968+00,
54. 5.906967+00, 6.003927+00, 6.103286+00, 6.205074+00, 6.309415+00, 6.416321+00,
55. 6.525873+00, 6.638005+00, 6.752699+00, 6.869801+00, 6.989183+00, 7.110780+00,
56. 7.234488+00, 7.360109+00, 7.487697+00, 7.617462+00, 7.749263+00, 7.883043+00,
57. 8.019027+00, 8.157287+00, 8.298187+00, 8.441755+00, 8.588284+00, 8.738131+00,
58. 8.891336+00, 9.047753+00, 9.207730+00, 9.371195+00, 9.538828+00, 9.710073+00,
59. 9.885916+00, 1.006370+01, 1.024686+01, 1.043356+01, 1.062451+01, 1.081977+01,
60. 1.101893+01, 1.122277+01, 1.143118+01, 1.164336+01, 1.186112+01, 1.208241+01,
61. 1.230957+01, 1.254034+01, 1.277702+01, 1.301752+01, 1.326369+01, 1.351482+01,
62. 1.377124+01, 1.403298+01, 1.429982+01, 1.457224+01, 1.485039+01, 1.513370+01,

```

63.	1.542333+01,	1.571868+01,	1.601991+01,	1.632718+01,	1.664108+01,	1.696098+01,
64.	1.728794+01,	1.762048+01,	1.796002+01,	1.833654+01,	1.866032+01,	1.902024+01,
65.	1.938760+01,	1.776240+01,	2.014479+01,	2.053477+01,	2.093249+01,	2.133799+01,
66.	2.175140+01,	2.217280+01,	2.250293+01,	2.304184+01,	2.348920+01,	2.352260+01,
67.	Y1A9(1)=1.732051, 1.732051, 1.732051, 1.725721, 1.627836, 1.460524, 1.354854,					
68.	1.284408,	1.143514,	1.074717,	1.027053,	1.012336,	1.00057,
69.	1.000000+00, 1.000047+00, 1.000193+00, 1.000446+00, 1.000814+00,					
70.	1.001304+00,	1.001922+00,	1.002678+00,	1.003579+00,	1.004635+00,	1.005854+00,
71.	1.007247+00,	1.008824+00,	1.010596+00,	1.012576+00,	1.014779+00,	1.017218+00,
72.	1.019912+00,	1.022879+00,	1.026139+00,	1.029718+00,	1.033641+00,	1.037939+00,
73.	1.042648+00,	1.047810+00,	1.053470+00,	1.059659+00,	1.066530+00,	1.074078+00,
74.	1.082501+00,	1.091040+00,	1.099451+00,	1.107359+00,	1.116284+00,	1.124712+00,
75.	1.133157+00,	1.141589+00,	1.150005+00,	1.158446+00,	1.166860+00,	1.175318+00,
76.	1.183745+00,	1.192209+00,	1.200684+00,	1.209154+00,	1.217668+00,	1.226151+00,
77.	1.234677+00,	1.243220+00,	1.251750+00,	1.260345+00,	1.268888+00,	1.277485+00,
78.	1.286120+00,	1.294720+00,	1.303374+00,	1.312056+00,	1.320719+00,	1.329436+00,
79.	1.338174+00,	1.346905+00,	1.355690+00,	1.364493+00,	1.373298+00,	1.382158+00,
80.	1.391032+00,	1.399916+00,	1.408856+00,	1.417809+00,	1.426776+00,	1.435801+00,
81.	1.444040+00,	1.453895+00,	1.463010+00,	1.473170+00,	1.483347+00,	1.493607+00,
82.	1.503831+00,	1.514146+00,	1.524521+00,	1.534978+00,	1.545325+00,	1.555821+00,
83.	1.566319+00,	1.576906+00,	1.587531+00,	1.598175+00,	1.608909+00,	1.619669+00,
84.	1.630467+00,	1.641379+00,	1.652239+00,	1.663209+00,	1.674271+00,	1.685293+00,
85.	1.696427+00,	1.707643+00,	1.718835+00,	1.730139+00,	1.741516+00,	1.752884+00,
86.	1.764364+00,	1.775910+00,	1.787460+00,	1.799123+00,	1.810843+00,	1.822583+00,
87.	1.834436+00,	1.846335+00,	1.858272+00,	1.870321+00,	1.882406+00,	1.894547+00,
88.	1.906799+00,	1.919074+00,	1.931427+00,	1.943911+00,	1.956345+00,	1.967748+00,
89.	1.978109+00,	1.988467+00,	1.998845+00,	2.009293+00,	2.019783+00,	2.030227+00,
90.	2.040762+00,	2.051351+00,	2.061931+00,	2.072535+00,	2.083214+00,	2.093939+00,
91.	2.104617+00,	2.115391+00,	2.126224+00,	2.137050+00,	2.147900+00,	2.158833+00,
92.	2.169914+00,	2.180746+00,	2.191781+00,	2.202879+00,	2.213971+00,	2.225091+00,
93.	2.236297+00,	2.247555+00,	2.258762+00,	2.270078+00,	2.281507+00,	2.292804+00,
94.	2.304232+00,	2.315729+00,	2.327276+00,	2.338977+00,	2.350390+00,	2.362116+00,
95.	2.373714+00,	2.385446+00,	2.397253+00,	2.409099+00,	2.420913+00,	2.432842+00,
96.	2.444873+00,	2.456789+00,	2.468842+00,	2.480972+00,	2.493124+00,	2.505268+00,
97.	2.517524+00,	2.529863+00,	2.542113+00,	2.554497+00,	2.566963+00,	2.579419+00,
98.	2.591906+00,	2.604501+00,	2.617145+00,	2.629742+00,	2.642468+00,	2.655301+00,
99.	2.668009+00,	2.680866+00,	2.693807+00,	2.706748+00,	2.719704+00,	2.732778+00,
100.	2.745906+00,	2.758976+00,	2.772180+00,	2.785495+00,	2.798867+00,	2.812014+00,
101.	2.825439+00,	2.838847+00,	2.852287+00,	2.865343+00,	2.879432+00,	2.892986+00,
102.	2.906672+00,	2.920441+00,	2.934110+00,	2.947925+00,	2.961873+00,	2.975655+00,
103.	2.989599+00,	3.003635+00,	3.017649+00,	3.031693+00,	3.045855+00,	3.060038+00,
104.	3.074196+00,	3.088484+00,	3.102834+00,	3.117135+00,	3.131518+00,	3.146031+00,
105.	3.160418+00,	3.174955+00,	3.189630+00,	3.204135+00,	3.218796+00,	3.233553+00,
106.	3.248262+00,	3.263031+00,	3.277916+00,	3.292784+00,	3.307685+00,	3.322713+00,
107.	3.337769+00,	3.368207+00,	3.399030+00,	3.430466+00,	3.462328+00,	3.494592+00,
108.	3.527437+00,	3.560757+00,	3.594396+00,	3.628521+00,	3.663422+00,	3.698580+00,
109.	3.734159+00,	3.770306+00,	3.807013+00,	3.844056+00,	3.881509+00,	3.919508+00,
110.	3.958049+00,	3.997024+00,	4.036284+00,	4.076077+00,	4.116400+00,	4.157254+00,
111.	4.198639+00,	4.240380+00,	4.282610+00,	4.325402+00,	4.368780+00,	4.412786+00,
112.	4.457331+00,	4.502545+00,	4.548471+00,	4.595102+00,	4.642591+00,	4.690797+00,
113.	4.739769+00,	4.789453+00,	4.839813+00,	4.890759+00,	4.942211+00,	4.994121+00,
114.	5.046424+00,	5.099019+00,	5.151910+00,	5.205168+00,	5.258715+00,	5.312512+00,
115.	5.366631+00,	5.421082+00,	5.475932+00,	5.531205+00,	5.586984+00,	5.643386+00,
116.	5.700388+00,	5.757903+00,	5.815929+00,	5.874483+00,	5.933782+00,	5.993590+00,
117.	6.053776+00,	6.114419+00,	6.175748+00,	6.237332+00,	6.299329+00,	6.361835+00,
118.	6.424513+00,	6.487705+00,	6.551260+00,	6.614856+00,	6.679095+00,	6.743151+00,
119.	6.807919+00,	6.872217+00,	6.937106+00,	7.001699+00,	7.066552+00,	7.131360+00,
120.	7.196123+00,	7.260897+00,	7.325375+00,	7.389772+00,	7.454065+00,	7.517884+00,
121.	7.581598+00,	7.644993+00,	7.707951+00,	7.770439+00,	7.832558+00,	7.894100+00,
122.	7.955182+00,	8.015377+00,	8.074924+00,	8.133751+00,	8.191821+00,	8.248870+00,
123.	8.305030+00,	8.360216+00,	8.414355+00,	8.467353+00,	8.519138+00,	8.569623+00,
124.	8.618737+00,	8.666398+00,	8.712597+00,	8.757247+00,	8.800224+00,	8.803367+00,
125.	P1A9(1)=1.0,					
126.	.9993289+00, .9968773+00, .9883995+00, .9813572+00,					
127.	.9560030+00,	.9299963+00,	.8910000+00,	.8344955+00,	.8029922+00,	
128.	.7699944+00,	.6719799+00,	.4690063+00,	.3939462+00,	.3782794+00,	
129.	.3629402+00,	.3478886+00,	.3330965+00,	.3185543+00,	.3042776+00,	

130.	.2902278+00,	.2764128+00,	.2628242+00,	.2474565+00,	.2363410+00,
131.	.2234505+00,	.2107971+00,	.1983850+00,	.1862244+00,	.1743224+00,
132.	.1626801+00,	.1513146+00,	.1402307+00,	.1294374+00,	.1189491+00,
133.	.1087770+00,	.9893494-01,	.8943256-01,	.8023729-01,	.7151720-01,
134.	.6313558-01,	.5516107-01,	.5070982-01,	.5035799-01,	.5010706-01,
135.	.4976724-01,	.4947381-01,	.4913162-01,	.4878817-01,	.4877959-01,
136.	.4845610-01,	.4840110-01,	.4805607-01,	.4791657-01,	.4756982-01,
137.	.4722082-01,	.4707443-01,	.4672511-01,	.4659512-01,	.4624500-01,
138.	.4589290-01,	.4578011-01,	.4542807-01,	.4532850-01,	.4497600-01,
139.	.4462136-01,	.4452357-01,	.4416952-01,	.4381375-01,	.4371584-01,
140.	.4336062-01,	.4300399-01,	.4290566-01,	.4254953-01,	.4219238-01,
141.	.4209341-01,	.4173674-01,	.4137928-01,	.4128026-01,	.4092337-01,
142.	.4056591-01,	.4046910-01,	.4011234-01,	.3975515-01,	.3966070-01,
143.	.3930432-01,	.3894769-01,	.3881508-01,	.3841962-01,	.3829038-01,
144.	.3789626-01,	.3750164-01,	.3737501-01,	.3696225-01,	.3658935-01,
145.	.3646531-01,	.3607424-01,	.3568336-01,	.3556163-01,	.3517260-01,
146.	.3478407-01,	.3466451-01,	.3427786-01,	.3415392-01,	.3377541-01,
147.	.3339196-01,	.3327528-01,	.3289362-01,	.3251237-01,	.3239881-01,
148.	.3202028-01,	.3164240-01,	.3153108-01,	.3115596-01,	.3078171-01,
149.	.3067260-01,	.3030111-01,	.2993072-01,	.2982396-01,	.2945637-01,
150.	.2909004-01,	.2898557-01,	.2862208-01,	.2826004-01,	.2815797-01,
151.	.2779875-01,	.2744120-01,	.2734140-01,	.2698566-01,	.2688823-01,
152.	.2653674-01,	.2621366-01,	.2591793-01,	.2587523-01,	.2558200-01,
153.	.2529023-01,	.2524974-01,	.2496085-01,	.2467323-01,	.2438749-01,
154.	.2434995-01,	.2406686-01,	.2378537-01,	.2374999-01,	.2347142-01,
155.	.2319425-01,	.2291899-01,	.2288647-01,	.2261393-01,	.2234306-01,
156.	.2231228-01,	.2204437-01,	.2177793-01,	.2151346-01,	.2148132-01,
157.	.2121962-01,	.2095966-01,	.2093349-01,	.2067650-01,	.2042105-01,
158.	.2039652-01,	.2014424-01,	.1989334-01,	.1964445-01,	.1962106-01,
159.	.1937512-01,	.1913081-01,	.1910794-01,	.1886674-01,	.1862703-01,
160.	.1838933-01,	.1836896-01,	.1813416-01,	.1790107-01,	.1786262-01,
161.	.1765257-01,	.1742403-01,	.1719763-01,	.1716185-01,	.1695820-01,
162.	.1673634-01,	.1672241-01,	.1650346-01,	.1628519-01,	.1607093-01,
163.	.1605959-01,	.1584703-01,	.1563633-01,	.1562675-01,	.1541882-01,
164.	.1521266-01,	.1520482-01,	.1500148-01,	.1479983-01,	.1460015-01,
165.	.1459472-01,	.1439767-01,	.1420247-01,	.1419567-01,	.1400612-01,
166.	.1381535-01,	.1381313-01,	.1362502-01,	.1343864-01,	.1325410-01,
167.	.1325422-01,	.1307226-01,	.1289213-01,	.1289367-01,	.1271603-01,
168.	.1254018-01,	.1254319-01,	.1236980-01,	.1219818-01,	.1220253-01,
169.	.1203333-01,	.1186587-01,	.1170025-01,	.1170664-01,	.1154531-01,
170.	.1138178-01,	.1138942-01,	.1123012-01,	.1107261-01,	.1108152-01,
171.	.1092617-01,	.1077260-01,	.1078267-01,	.1063115-01,	.1048144-01,
172.	.1049259-01,	.1034480-01,	.1019885-01,	.1005458-01,	.1006729-01,
173.	.9924930-02,	.9784270-02,	.9797875-02,	.9658920-02,	.9521635-02,
174.	.9535710-02,	.9264285-02,	.9143167-02,	.9021952-02,	.8756996-02,
175.	.8637295-02,	.8517986-02,	.8260701-02,	.8143489-02,	.8026902-02,
176.	.7910104-02,	.7862924-02,	.7548961-02,	.7435734-02,	.7322693-02,
177.	.7086801-02,	.6977633-02,	.6869901-02,	.6762943-02,	.6538982-02,
178.	.6435813-02,	.6334363-02,	.6233711-02,	.6133379-02,	.6034801-02,
179.	.5826943-02,	.5731683-02,	.5636894-02,	.5542659-02,	.5448765-02,
180.	.5355157-02,	.5262225-02,	.5169365-02,	.5076380-02,	.4983142-02,
181.	.4809821-02,	.4796453-02,	.4703356-02,	.4610705-02,	.4518904-02,
182.	.4428248-02,	.4338923-02,	.4251115-02,	.4165120-02,	.4080842-02,
183.	.3993379-02,	.3916921-02,	.3837061-02,	.3758551-02,	.3681569-02,
184.	.3681789-02,	.3605872-02,	.3530771-02,	.3456608-02,	.3382521-02,
185.	.3309336-02,	.3306768-02,	.3233617-02,	.3160939-02,	.3088585-02,
186.	.3083052-02,	.3011104-02,	.2939805-02,	.2932064-02,	.2860762-02,
187.	.2790575-02,	.2780556-02,	.2710681-02,	.2698526-02,	.2620761-02,
188.	.2615975-02,	.2546929-02,	.2533571-02,	.2465431-02,	.2451545-02,
189.	.2384562-02,	.2370067-02,	.2304422-02,	.2293939-02,	.2272856-02,
190.	.2207800-02,	.2191073-02,	.2127079-02,	.2109429-02,	.2090706-02,
191.	.2071597-02,	.2009000-02,	.1990027-02,	.1970350-02,	.1950389-02,
192.	.1929964-02,	.1869390-02,	.1848887-02,	.1827909-02,	.1806022-02,
193.	.1783568-02,	.1761031-02,	.1738138-02,	.1715018-02,	.1691699-02,
194.	.1668181-02,	.1644484-02,	.1620599-02,	.1596546-02,	.1572334-02,
195.	.1547700-02,	.1522649-02,	.1516203-02,	.0000000	.0000000
196.	SEND				

197.	12							04100	A
198.	0.0	.002	.006	.01	.025	.06	.15	04201	A
199.	.4	.7	1.0	1.5	2.5			04202	A
200.	10	.95	1 3 0.5					04300	A
201.	0.0	.05	.12	.25	.35	.45	.6	04401	A
202.	.75	.85	.95	.98	1.0			04402	A
203.	.014351							05100	A
204.	1.02732+06							07100	A
205.	4.18650+04							07200	A
206.	0.0							07300	A
207.	.44	11.823	.018	.9	.9	600.		08100	A
208.	3.3909+05							09600	A
209.	2							11100	A
210.	N NITROGEN	14.008	-.768					11201	A
211.	O OXYGEN	16.0	-.232					11202	A
212.	100.	1000.	5000.					13100	A
213.	N2 COLD AIR	NONE	N 2		.6 100.	5000.			1
214.	3.51515								2
215.	-1054.545	6.08115		3.51515					3
216.				-1054.545	6.08115				4
217.	O2 COLD AIR	NONE	O 2		.6 100.	5000.			1
218.	3.53								2
219.	-1059.09	6.06489		3.53					3
220.				-1059.09	6.06489				4
221.								13LAST	
222.								15201	A
223.								15202	A
224.								15203	A
225.								15204	A
226.	294.4	294.4	294.4	294.4	294.4	294.4	294.4	16201	A
227.	294.4	294.4	294.4	294.4	294.4	294.4	294.4	16202	A
228.	294.4	294.4	294.4	294.4	294.4	294.4	294.4	16203	A
229.	294.4	294.4	294.4	294.4	294.4	294.4		16204	A
230.								16601	A
231.								16602	A
232.								16603	A
233.								16604	A
234.								16605	A
235.								16606	A
236.								16607	A
237.								16608	A
238.								16609	A
239.								16610	A
240.								16611	A
241.								16612	A
242.								LAST	A

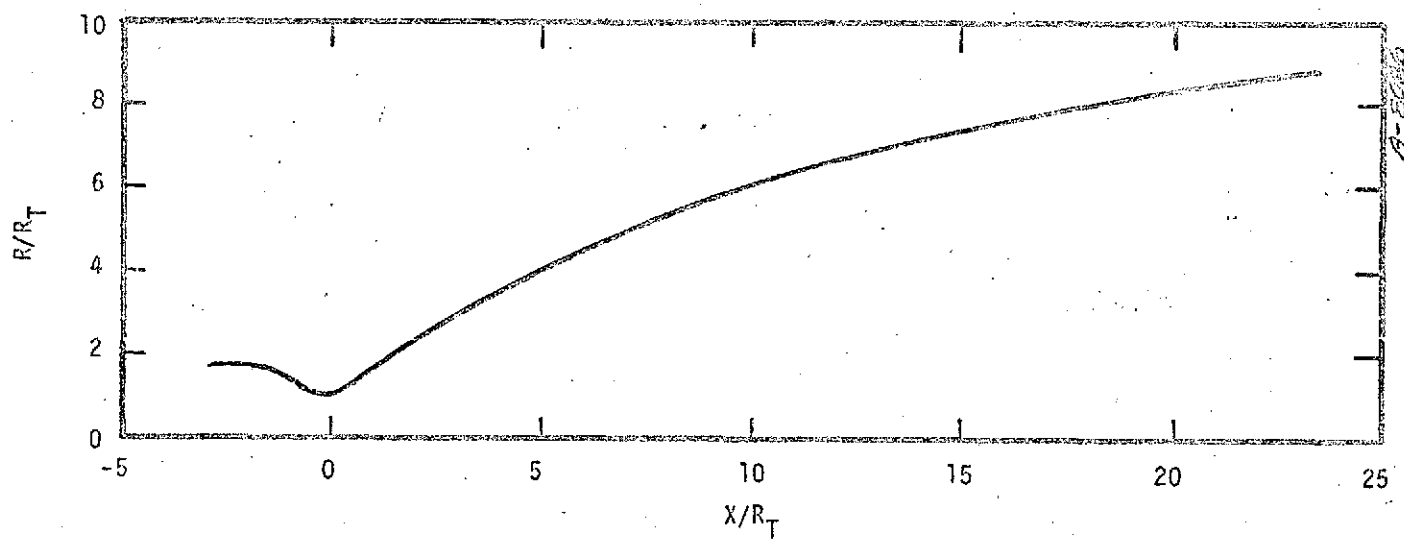


Figure A-2. SSME Model Nozzle Contour

Area Ratio = 77.5

Length = 0.376 m (14.825 in)

$R_T = 0.014351$ m (0.565 in)

A.3 INPUT DATA FOR BACK AND CUFFEL PREDICTIONS

1.	10100420210212000000	JPL DATA	AIR CARDS					01100	J
2.	2							02100	J
3.	24							03100	J
4.	0.01	0.05	0.1	0.2	0.4	1.0	2.0	03201	J
5.	3.761	3.417	4.107	4.234	4.361	4.488	4.575	03202	J
6.	4.609	4.633	4.647	4.676	4.720	4.781	4.907	03203	J
7.	5.063	5.258	5.374					03204	J
8.	13							04100	J
9.	0.0	0.002	0.006	0.01	0.025	0.06	0.15	04201	J
10.	0.4	0.7	1.0	1.5	2.5	4.0		04202	J
11.	10.0.95	1.3	.5					04300	J
12.	0.0	0.05	0.12	0.25	0.35	0.45	0.6	04401	J
13.	0.75	0.875	0.95	0.985	0.99	1.0		04402	J
14.	1.0							05100	J
15.	.20833	.20833	.20833	.20833	.20833	.20833	.20833	05201	J
16.	.20833	.1925	.1592	.1374	.1153	.09325	.07833	05202	J
17.	.07233	.06817	.06665	.06708	.0745	.08517	.10708	05203	J
18.	.134	.1685	.189					05204	J
19.	10.21							07100	J
20.	240.97							07200	J
21.	0.0							07300	J
22.	0.44	11.82	0.018	0.9	0.9			08100	J
23.	36.74							09600	J
24.	2							11101	J
25.	N NITROGEN	14.008	.768					11201	J
26.	O OXYGEN	16.0	.232					11202	J
27.	100.	1000.	5000.					13100	J
28.	N2 COLD AIR	NONE	N 2		G 100.	5000.		1	
29.	3.51515							2	
30.	-1054.545	6.08115		3.51515				3	
31.				-1054.545	6.08115			4	
32.	O2 COLD AIR	NONE	O 2		G 100.	5000.		1	
33.	3.53							2	
34.	-1059.09	6.06489		3.53				3	
35.				-1059.09	6.06489			4	
36.								13LAST	
37.	0.9972	0.9972	0.9972	0.9972	0.9972	0.9972	0.9972	15101	J
38.	0.9972	0.99635	0.99257	0.98703	0.9740	0.93704	0.8659	15102	J
39.	0.7807	0.6768	0.4987	0.3512	0.2317	0.1489	0.05927	15102	J
40.	0.02767	0.016555	0.01211						
41.								15201	J
42.								15202	J
43.								15203	J
44.								15204	J
45.	690.	690.	690.	690.	690.	690.	690.	16201	J
46.	690.	691.	707.	724.	743.	775.	823.	16202	J
47.	842.	810.	808.	789.	782.	758.	726.	16203	J
48.	693.	660.	649.					16204	J
49.								16601	J
50.								16602	J
51.								16603	J
52.								16604	J
53.								16605	J
54.								16606	J
55.								16607	J
56.								16608	J
57.								16609	J
58.								16610	J
59.								16611	J
60.								16612	J
61.								LAST	J